Acta Pharmaceutica Sinica B 2025;15(5):2593−2611

Chinese Pharmaceutical Association
Institute of Materia Medica, Chinese Academy of Medical Sciences

Acta Pharmaceutica Sinica B

www.elsevier.com/locate/apsb
www.sciencedirect.com

ORIGINAL ARTICLE

USP51/GRP78/ABCB1 axis confers chemoresistance through decreasing doxorubicin accumulation in triple-negative breast cancer cells

Yang Ou[a], Kun Zhang[a], Qiuying Shuai[a], Chenyang Wang[a], Huayu Hu[a], Lixia Cao[a], Chunchun Qi[a], Min Guo[a], Zhaoxian Li[a], Jie Shi[a], Yuxin Liu[a], Siyu Zuo[a], Xiao Chen[a], Yanjing Wang[a], Mengdan Feng[a], Hang Wang[a], Peiqing Sun[b], Yi Shi[a,*], Guang Yang[a,*], Shuang Yang[a,*]

[a]*Tianjin Key Laboratory of Tumor Microenvironment and Neurovascular Regulation, School of Medicine, College of Pharmacy, Nankai University, Tianjin 300071, China*
[b]*Department of Cancer Biology, Wake Forest University School of Medicine, Winston-Salem, NC 27157, USA*

Received 13 March 2024; received in revised form 24 June 2024; accepted 9 December 2024

KEY WORDS

TNBC;
USP51;
GRP78;
ABCB1;
Chemoresistance;
Doxorubicin;
Deubiquitinating enzyme;
Inhibitor

Abstract Recent studies have indicated that the expression of ubiquitin-specific protease 51 (USP51), a novel deubiquitinating enzyme (DUB) that mediates protein degradation as part of the ubiquitin−proteasome system (UPS), is associated with tumor progression and therapeutic resistance in multiple malignancies. However, the underlying mechanisms and signaling networks involved in USP51-mediated regulation of malignant phenotypes remain largely unknown. The present study provides evidence of USP51's functions as the prominent DUB in chemoresistant triple-negative breast cancer (TNBC) cells. At the molecular level, ectopic expression of USP51 stabilized the 78 kDa Glucose-Regulated Protein (GRP78) protein through deubiquitination, thereby increasing its expression and localization on the cell surface. Furthermore, the upregulation of cell surface GRP78 increased the activity of ATP binding cassette subfamily B member 1 (ABCB1), the main efflux pump of doxorubicin (DOX), ultimately decreasing its accumulation in TNBC cells and promoting the development of drug resistance both *in vitro* and *in vivo*. Clinically, we found significant correlations among USP51, GRP78, and ABCB1 expression in TNBC patients with chemoresistance. Elevated USP51, GRP78, and ABCB1 levels were also strongly associated with a poor patient

*Corresponding authors.
E-mail addresses: yangshuang@nankai.edu.cn (Shuang Yang), guang.yang@nankai.edu.cn (Guang Yang), yishi@nankai.edu.cn (Yi Shi).
Peer review under the responsibility of Chinese Pharmaceutical Association and Institute of Materia Medica, Chinese Academy of Medical Sciences.

https://doi.org/10.1016/j.apsb.2025.03.004

prognosis. Importantly, we revealed an alternative intervention for specific pharmacological targeting of USP51 for TNBC cell chemosensitization. In conclusion, these findings collectively indicate that the USP51/GRP78/ABCB1 network is a key contributor to the malignant progression and chemotherapeutic resistance of TNBC cells, underscoring the pivotal role of USP51 as a novel therapeutic target for cancer management.

1. Introduction

Breast cancer is the most common malignancy worldwide. Triple-negative breast cancer (TNBC) accounts for 15%−20% of all breast cancer cases and often occurs in younger females[1-3]. Due to the lack of estrogen receptor, progesterone receptor, and human epidermal growth factor receptor expression, cytotoxic chemotherapy is currently the most effective intervention for patients with TNBC[4-6]. While an initial response is consistently observed among patients, the prognosis of TNBC remains poor due to chemotherapeutic resistance and tumor recurrence[3,7]. To overcome this obstacle, it is necessary to elucidate the critical molecular mechanisms of resistance to chemotherapy in TNBC and apply this information to develop effective chemosensitizers.

In addition to a variety of genetic and epigenetic mechanisms[8,9], recent studies have demonstrated that the dynamic modulation of protein homeostasis also plays a pivotal role in the regulation of TNBC chemoresistance[10-13]. One such dynamic modulator is the ubiquitin−proteasome system (UPS), which modulates the stability and activity of target proteins through the coordination of ubiquitination and deubiquitination[14,15]. For example, TNBC exhibits a high level of genome instability and an inefficient DNA damage response (DDR), which is a major cause of chemotherapy failure[16,17]. The DDR, especially the ubiquitination of histone proteins, is tightly controlled by the UPS[18-20]. In this process, treatment with chemotherapeutic drugs induces DNA strand breaks, which promote the recruitment of core components of the UPS, such as ring finger protein 8 (RNF8) and RNF168, to increase the protein stability of histones H1 and H2A through ubiquitination, eventually resulting in increased DNA end resection and an aberrant response to chemotherapy in cancer cells[21,22]. Moreover, a growing body of evidence has shown that the UPS regulates the activity of epithelial−mesenchymal transition (EMT)-associated transcription factors linked to chemoresistance in TNBC[14,23]. For example, deubiquitinating enzyme 3 (DUB3), an essential enzyme in the UPS, has been reported to interact with and stabilize the EMT regulators Snail and Twist through deubiquitination, thereby reducing cancer cell sensitivity to chemotherapeutic drugs such as doxorubicin (DOX)[24-26]. Given that the expression and activity of core components of the UPS are closely associated with the chemotherapeutic response of patients with TNBC[27,28], a comprehensive understanding of the functions of the UPS and identification of effective interventions for treating breast cancer are vital.

Accordingly, the imbalance between ubiquitination and deubiquitination is a key mechanism that impairs protein homeostasis and triggers the pathological process of chemoresistance in TNBC cells[28,29]. Ubiquitination is a reversible posttranslational modification that covalently conjugates a ubiquitin (Ub) moiety onto a substrate molecule. This process may further regulate the activity, interaction, and stability of substrate proteins. Protein ubiquitination is constantly reversed by DUBs that remove Ub from substrates and therefore prevent their proteosome-dependent degradation[30,31]. Ubiquitin-specific protease 51 (USP51) is a novel DUB that functions in UPS-mediated protein degradation[19,32,33]. Increasing evidence has demonstrated a correlation between the dysregulation of USP51 and chemotherapeutic resistance in multiple malignancies[34-39]. For example, USP51 can promote the deubiquitination of histones to restrain abnormal DNA repair in response to chemotherapeutic drug treatment in TNBC and osteosarcoma cells[18,32,37]. Ectopic USP51 also contributes to the development of chemoresistance by deubiquitinating and stabilizing various EMT transcription factors, such as Zeb1 and Twist, in TNBC, gastric cancer, and non-small cell lung cancer[34,35,38,39]. Notably, elevated USP51 expression suggests a poor prognosis; therefore, it has been considered a marker for prognosis and a potential target for anticancer drugs[33-35,39,40]. Further identification of the molecular mechanisms that confer USP51 dysregulation may aid in the development of novel and efficacious drugs to decrease USP51 content and eventually overcome therapeutic resistance and decrease the malignancy of human cancers.

The present study provides evidence that, at the molecular level, USP51 functions as the prominent DUB in chemoresistant TNBC cells. Our investigation revealed that ectopically expressed USP51 stabilizes 78 kDa glucose-regulated protein (GRP78) through deubiquitination, thereby increasing GRP78 expression on the cell surface. Furthermore, the upregulation of cell surface GRP78 increases the activity of ATP binding cassette subfamily B member 1 (ABCB1), the main efflux pump of DOX, ultimately leading to the development of chemoresistance both *in vitro* and *in vivo*. In addition, our results revealed that pharmacologically targeting USP51 in breast cancer increases chemotherapeutic sensitivity. Overall, the present study demonstrated a significant correlation between impairment of the USP51/GRP78 axis and DOX resistance that is related to an ABCB1-dependent mechanism, underscoring the potential role of USP51 as a novel therapeutic target for cancer management.

2. Materials and methods

2.1. Cell culture

The human TNBC cell line MDA-MB-231, the human embryonic kidney cell line 293T and the human ovarian cancer cell line HeLa were obtained from the American Type Culture Collection (Manassas, VA, USA). DOX-resistant MDA-MB-231^{R} cells were

established by exposing parental MDA-MB-231 cells to a step-by-step increase in the DOX concentration from 10 to 100 nmol/L. The IC_{50} of MDA-MB-231^R cells was detected *via* a cell viability assay until the resistance index (RI) exceeded 5. The human TNBC cell line Cal51 and DOX-resistant Cal51^R cells were obtained from Tianjin Medical University Cancer Institute & Hospital (Tianjin, China). All the cells were confirmed to be mycoplasma negative with the GMyc-PCR Mycoplasma Detection Kit (Yeasen, Shanghai, China). MDA-MB-231 and Cal51 cells were cultured in RPMI-1640 containing 10% FBS and 1% penicillin−streptomycin. MDA-MB-231^R and Cal51^R cells were cultured in RPMI-1640 containing 10% FBS and 1% penicillin−streptomycin with 1 μmol/L or 100 nmol/L DOX, respectively. 293T and HeLa cells were cultured in DMEM containing 10% FBS and 1% penicillin−streptomycin.

2.2. Reagents

The concentration of cycloheximide (CHX) (Selleck, TX, USA) was 100 μg/mL. The doses of the chemotherapeutic drug DOX (TOPSCIENCE, Shanghai, China) were 1 μmol/L *in vitro* and 2 mg/kg *in vivo*. The proteasome inhibitor MG132 (Selleck, TX, USA) was used at a concentration of 20 μmol/L. The dose of the ABCB1 inhibitor Encequidar (TOPSCIENCE, Shanghai, China) was 100 nmol/L.

2.3. Lentivirus-mediated knockdown and expression

Specific short hairpin RNAs (shRNAs) for *USP51*, *MINDY1*, *OTUB2*, and *GRP78* underwent annealing and subcloning into the pLVH1-EF1α-puro vector (Biosettia, San Diego, CA, USA). The full-length *USP51* and *GRP78*, as well as related deletion constructs (Myc-USP51-N, Myc-USP51-C, Flag-GRP78-G1, Flag-GRP78-G2, Flag-GRP78-G3 and Flag-GRP78-G4), were subcloned and inserted into the pLV-EF1-MCS-IRES-Bsd vector (Biosettia). The individual mutants of *USP51* (C372S) and *GRP78* (K516R, K523R, K547R, K556R, K573R and K601R) were also subcloned and inserted into the pLVEF1-MCS-IRES-Bsd vector. The constructed and packaged plasmids, including gag polyprotein (Gag-Pol), the regulator of expression of virion protein (Rev), and vesicular stomatitis virus glycoprotein G (VSVG) (Biosettia) were then cotransfected into 293T cells with Lipofectamine 2000 reagent (Invitrogen, MA, USA) to produce lentivirus particles. The details of the primers used can be found in Supporting Information Table S1.

2.4. Western blotting analysis

Total protein isolation and Western blotting were conducted as reported previously[35]. Protein samples were obtained *via* cell incubation in radioimmunoprecipitation assay (RIPA) lysis buffer (Yeasen) with protease and phosphatase inhibitors (Yeasen), and then protein concentration was quantified with a bicinchoninic acid kit (ThermoFisher Scientific, MA, USA). Protein separation was performed *via* sodium dodecyl sulfate−polyacrylamide gel electrophoresis (SDS−PAGE), and the separated proteins were transferred to polyvinylidene fluoride membranes (Millipore, Billerica, MA, USA); then, the membranes were blocked for 1 h in 5% skim milk (Yeasen) at room temperature, incubated overnight with primary antibodies at 4 °C and subsequently incubated for 1 h with secondary antibodies at room temperature. Finally, enhanced chemiluminescence reagents (Yeasen) were used for protein visualization. A summary of the employed antibodies is available in Supporting Information Table S2.

2.5. In vivo deubiquitination assay

The cells were incubated with hemagglutinin (HA)−Ub and the previously described plasmids (4 μg) for 48 h and then treated with 20 μmol/L MG132 (Yeasen) for 12 h to inhibit ubiquitin proteasome-dependent dysregulation of the protein. The cell lysates were obtained *via* cell incubation in RIPA buffer (Yeasen) prior to overnight incubation with anti-Flag antibody or IgG at 4 °C. The resulting immunoprecipitates were analyzed *via* anti-HA-Tag antibody-mediated Western blotting. The details of the antibodies used can be found in Table S2.

2.6. In vitro deubiquitination assay

HA-Ub and Flag-GRP78 were coexpressed in HEK293 cells. After the cells were treated with 20 μmol/L MG132 for 12 h, ubiquitinated GRP78 was isolated *via* IP with an anti-Flag antibody. The recombinant USP51 protein was incubated with ubiquitinated GRP78 in deubiquitination reaction buffer (50 mmol/L HEPES, pH 7.5, 100 mmol/L NaCl, 5% glycerol, 5 mmol/L $MgCl_2$, 1 mmol/L ATP and 1 mmol/L dithiothreitol (DTT)) at 30 °C for 30 min. The ubiquitination status of GRP78 was analyzed using an anti-HA-Tag antibody-mediated Western blotting.

2.7. Protein expression and purification of GRP78 proteins

Glutathione *S*-transferase (GST)-tagged GRP78 and its corresponding truncated mutants (GST-GRP78-G1, GST-GRP78-G2, GST-GRP78-G3 and GST-GRP78-G4) were cloned and inserted into the pGEX-6p-1 vector (Biosettia, San Diego, CA, USA) prior to expression in *E. coli* BL21 cells (WeiDi, Shanghai, China). For cell induction, 0.5 mmol/L isopropyl β-D-thiogalactopyranoside (IPTG) (Yeasen) in Luria−Bertani (LB) medium (Sigma, MI, USA) was used to treat cells at 16 °C for 24 h to induce GRP78 protein expression. Cell pellets were dissolved in lysis buffer (50 mmol/L Tris, 300 mmol/L NaCl), and 2 mg/mL lysozyme (Yeasen) was added and incubated at 4 °C overnight, followed by ultrasonication using an ultrasonic cell crusher (SCIENTZ, Zhejiang, China) and a 20 min centrifugation at 18,000 × *g* at 4 °C. Following the removal of the supernatant, the pellets were resuspended in solubilization buffer (200 mmol/L Tris, 5 mmol/L DTT, 8 mol/L urea, pH = 8.0). The insoluble material was centrifuged at 18,000 × *g* for 20 min at 4 °C and removed, and the supernatant was placed onto Glutathione Sepharose 4B beads (ThermoFisher Scientific) and equilibrated with binding buffer (50 mmol/L Tris, 300 mmol/L NaCl) overnight. The protein was eluted with elution buffer (50 mmol/L Tris, 300 mmol/L NaCl, and 10 mmol/L glutathione, pH = 7.5−8.0) and stored at −80 °C.

2.8. Coimmunoprecipitation (Co-IP) and GST pulldown assays

The cell lysates were obtained *via* cell incubation in RIPA buffer, incubated with the desired antibody or IgG at 4 °C overnight, and subsequently incubated with protein G resin (GenScript, Nanjing, China) for 4 h. Finally, the immunoprecipitates were separated *via* Western blotting with the corresponding antibodies. The details for the antibodies used can be found in Table S2.

2.9. In vitro binding assays

The purified proteins of histidine (His)-USP51 and GST-GRP78 (full-length GRP78 and its corresponding truncated mutants) were incubated at 4 °C overnight. Glutathione Sepharose 4B beads were added and incubated for 4 h before Western blotting of the bound proteins with a USP51 antibody (H00158880-A01, Abnova, Taiwan, China).

2.10. In vitro USP51 activity assay

The C-terminal conjugate of Ub with 7-amino-4-methylcoumarin (Ub-AMC) was used to measure the deubiquitinase activity of USP51. Briefly, the reaction system contained 50 mmol/L 2-hydroxyethyl, 0.5 mmol/L ethylene diamine tetraacetic acid, 100 mmol/L NaCl, 1 mmol/L DTT, 0.1 mg/mL bovine serum albumin, 250 nmol/L Ub-AMC (U-550, Boston Biochem, CA, USA), and the compounds were mixed. Then, 64 nmol/L USP51 (MERRYBIO, Nanjing, China) was added, and the fluorescence intensity was detected using a microplate reader (BMG Labtech, Offenburg, Germany) with a 345 nm excitation/460 nm emission optic module for 2 h. All the experiments included three biological replicates, and the mean value was analyzed.

2.11. Surface plasmon resonance (SPR)

The binding kinetic evaluations were conducted on a Biacore T200 (GE Healthcare, MA, USA). Briefly, His-tagged USP51 was immobilized in Acetate 4.0 (BR-1003-49, GE Healthcare) on a Biacore Series S NTA chip (CM5) *via* N-terminal His tag capture, followed by amine coupling with 1-(3-dimethylaminopropyl)-3-ethylcarbodiimide hydrochloride/*N*-hydroxy succinimide/ethanolamine (Sigma, MO, USA) as per the kit guidelines. A 7500-response unit immobilization was attempted. The compounds were examined in a 2-fold dilution series in immobilization buffer containing 5% (*v*/*v*) dimethylsulfoxide (DMSO) at 30 μL/min, with a 60 s contact time and a 120 s dissociation time. We also included a solvent correction curve between 4.5% and 5.8% (*v*/*v*) DMSO. Ten-point dilution curves before and after compounds were used to confirm surface integrity throughout the experiment. Biacore T200 evaluation software (version 3.0, GE Healthcare) was used for kinetic fitting.

2.12. Cellular thermal shift assay

The cells were subjected to 5 h of WCY-4-1 treatment at the specified concentrations. Then, the mixture was incubated for 3 min in PBS with a complete protease inhibitor cocktail and then incubated at 40, 43, 46 or 49 °C. Next, the cells were freeze−thawed in liquid nitrogen, and the supernatant was collected. Finally, proteins were assessed *via* Western blotting with a USP51 antibody (H00158880-A01; Abnova).

2.13. Cell viability assessment

A total of 3000 cells/well were plated in 96-well plates and treated with different drugs for the indicated durations. Cell survival was assessed *via* Cell Counting Kit-8 (Yeasen) assays as per the kit guidelines, and absorbance at 450 nm was detected *via* a microplate reader (BMG Labtech).

2.14. Colony formation experiment

Five hundred cells/well were plated in 6-well plates before treatment with different drugs for 10 days. The cells were fixed for 30 min in 4% paraformaldehyde (Sigma) and subjected to crystal violet staining for 15 min. The number of colonies was counted according to Eq. (1):

$$\text{Colony formation rate} = \text{colony number/plated cell number} \quad (1)$$

2.15. TdT-mediated dUTP nick-end labeling (TUNEL)

Cell apoptosis was detected using a TUNEL staining kit (Yeasen). Three random microscopic fields per slide were examined under a BX53 microscope (Olympus, Tokyo, Japan). The percentage of apoptotic cells was quantified as Eq. (2):

$$\begin{aligned}&\text{Percentage of apoptotic cells } (\%) = \\ &\quad \text{TUNEL}^{+} \text{ cell number}/4',6-\text{diamidino2} \\ &\quad -\text{phenylindole } (\text{DAPI})^{+} \text{ cell number} \times 100\end{aligned} \quad (2)$$

2.16. Immunofluorescence assay

The cells were subjected to 24-h treatment with various drugs before fixation in 4% paraformaldehyde, followed by overnight incubation with a phosphorylated histone H2AX (γH2AX) antibody (Cell Signaling Technology, MA, USA) at 4 °C. The next day, the cells were treated for 1 h with a DyLight 488-conjugated secondary antibody (Abcam, Cambridge, UK) before 3 min of staining with DAPI (1 μg/mL). The labeled nuclei were detected on a confocal FV1000 microscope (Olympus, Tokyo, Japan). The percentage of cells with ≥10 foci was quantified. At least 100 cells were counted per well.

2.17. Tumor xenograft experiment

All animal protocols received ethical approval from the Medical College of Nankai University (2022-SYDWLL-000096). We obtained 6-week-old male NOD-SCID mice from Beijing HFK Bioscience Ltd. (Beijing, China). A total of 5×10^6 cells were subcutaneously implanted into the mammary fat pads. Once the tumors reached a volume of 50 mm^3, the mice were randomly divided into two groups with 5 mice per group. The mice were intraperitoneally injected with DOX (2 mg/kg in DMSO) and/or WCY-4-1 (2 mg/kg in DMSO) every other day and were sacrificed 3 weeks post-implantation. The tumors were weighed, and the volume was calculated as Eq. (3):

$$\text{Tumor volume} = 1/2\left(\text{Length} \times \text{Width}^2\right) \quad (3)$$

2.18. Patient tissue collection and immunohistochemistry (IHC) analysis

Samples were obtained from a total of 116 breast cancer patients who received anthracycline-based neoadjuvant chemotherapy at the General Hospital of the People's Liberation Army (Beijing, China) and the First Affiliated Hospital of Chongqing Medical University (Chongqing, China). The subjects were divided into two groups on the basis of the response evaluation criteria for

solid tumors [(non-resistance: complete response (CR), resistance: progressive disease (PD)] or Miller−Payne grade (non-resistance: grade 3−5, resistance: grade 1, 2). The samples were subjected to IHC staining for USP51, GRP78 (Proteintech, China) and ABCB1 (Proteintech) with the corresponding antibodies and the Envision Kit (ZSGB-Bio, China) in accordance with the kit protocols. Immunostaining was independently evaluated by two pathologists. The IHC scores were calculated by combining the quantity score (the percentage of positively stained cells in the evaluated area) with the staining intensity score. The quantity score ranged from 0 to 4: 0, no immunostaining; 1, 1%−14% positively stained cells; 2, 15%−49% positively stained cells; 3, 50%−74% positively stained cells; and 4, ≥75% positively stained cells. The staining intensity was scored as follows: 0 (no color), 1 (light yellow), 2 (light brown), 3 (brown), and 4 (dark brown). The total score for each tissue was calculated by summing the intensity and quantity scores (the range for the total score was therefore 0−8). Samples with an IHC score >4 were classified as having high expression, and those with an IHC score ≤4 were classified as having low expression. This protocol received ethical approval from Nankai University (NKUIRB2024059). The tissue samples were obtained with written informed consent from each patient. The clinicopathologic features of the breast tumors are listed in Supporting Information Tables 3 and 4.

2.19. Statistical analysis

The experimental data were analyzed with GraphPad Prism 8.0 (GraphPad Software, California, USA) and SPSS 17.0 (IBM, Illinois, USA) software. The data for all the experiments are expressed as the means ± standard deviation (SD) of three distinct replicates. Gene profile correlations in various samples were assessed *via* Spearman's rank correlation test. Intergroup comparisons were performed *via* one-way analysis of variance. Unpaired data assessments were conducted *via* Student's *t*-test, as appropriate. P value < 0.05 was set as the significance threshold.

3. Results

3.1. Ectopic USP51 plays a pivotal role in TNBC chemoresistance

To investigate the potential function of protein homeostasis regulated by ubiquitination in TNBC chemoresistance, we assessed the expression of polyubiquitinated proteins in both wild-type Cal51 and chemoresistant Cal51^R cells using an FK1 antibody. The results of Western blotting indicated that DOX treatment significantly increased the expression level of polyubiquitinated proteins in Cal51 cells; however, this effect was weakened in Cal51^R cells (Fig. 1A). Notably, RNA-sequencing analysis revealed that three DUBs were highly expressed in Cal51^R cells: MIU-containing novel DUB family member 1 (MINDY1), OTU domain-containing ubiquitin aldehyde-binding protein 2 (OTUB2), and USP51 (Fig. 1B). The upregulation of these DUBs at the mRNA and protein levels was further confirmed by qPCR (Fig. 1C) and Western blotting (Fig. 1D) of samples from Cal51^R cells and Cal51 cells as the control. Additionally, we established stable Cal51^R cell lines with specific knockdown of MINDY1 (Fig. 1E), OTUB2 (Fig. 1F), and USP51 (Fig. 1G). The results of cell viability analysis demonstrated that specific knockdown of USP51 significantly decreased the half-maximal inhibitory concentration (IC_{50}) of DOX in Cal51^R cells, whereas this effect was not observed with knockdown of MINDY1 or OTUB2 (Fig. 1H). Consistent with these findings, Western blotting analysis revealed a significant increase in the accumulation of polyubiquitinated proteins upon DOX treatment in shUSP51/Cal51^R cells (Fig. 1I). These experiments were also performed in MDA-MB-231^R cells, and similar results were obtained (Supporting Information Fig. S1).

Moreover, colony formation (Fig. 1J) and cell apoptosis (Fig. 1K) assays revealed that USP51 depletion effectively enhanced DOX-induced suppression of cell proliferation and promotion of cell apoptosis. Similarly, the expression of the antiapoptotic protein Bcl2 was significantly reduced in shUSP51/Cal51^R cells in response to DOX treatment, whereas the expression of the proapoptotic protein Bax was increased (Fig. 1L). We also investigated the effect of USP51 on the DOX-induced expression of γH2AX, which is a marker for monitoring the DDR[41]. Our findings revealed that USP51 knockdown strongly increased the number of γH2AX foci and the level of γH2AX expression upon DOX treatment (Fig. 1M and N). Similar results were also obtained in shUSP51/MDA-MB-231^R cells (Supporting Information Fig. S2), highlighting that USP51 might play an important role in the regulation of TNBC chemoresistance through a protein homeostasis-dependent mechanism.

3.2. USP51 promotes TNBC chemoresistance via its DUB activity

To further determine whether USP51 promotes TNBC chemoresistance through its DUB activity, we introduced wild-type USP51 and a catalytically inactive mutant USP51^{C372S} [32] into Cal51 cells (Fig. 2A). The results of the cell viability (Fig. 2B), colony formation (Fig. 2C), cell apoptosis (Fig. 2D and E), and DNA damage detection (Fig. 2F and G) assays revealed that overexpression of wild-type USP51 could reduce the sensitivity of Cal51 cells to DOX treatment, whereas these effects were strongly attenuated in USP51^{C372S}-expressing cells. We also performed these experiments in MDA-MB-231 cells and obtained the same results (Supporting Information Fig. S3), indicating that USP51 regulates TNBC cell chemosensitivity in a DUB activity-dependent manner.

Next, we sought to verify whether ectopic USP51 affects TNBC cell sensitivity to DOX *in vivo*. To do so, USP51/Cal51 and USP51^{C372S}/Cal51 cells were subcutaneously injected into Nod-SCID mice to establish xenograft models, and then DOX was administered intraperitoneally. The results confirmed that DOX strongly suppressed the development of Ctrl/Cal51-and USP51^{C372S}/Cal51 cell-derived tumors in mice (Fig. 2H), as tumor volume (Fig. 2I) and weight (Fig. 2J) were reduced by approximately 90%. However, this effect was not detected in mice engrafted with USP51/Cal51 cells. Immunohistochemical staining further demonstrated that DOX markedly reduced the expression of Ki67 but increased the expression of cleaved caspase-3 and γH2AX in Ctrl/Cal51 and USP51^{C372S}/Cal51 tumors, whereas these effects were not observed in USP51/Cal51 tumors (Fig. 2K). Taken together, these findings indicate a critical role for USP51 DUB activity in the chemotherapeutic response *in vivo* and *in vitro*.

3.3. USP51 deubiquitinates and stabilizes GRP78

To identify potential target proteins of USP51, endogenous Co-IP combined with mass spectrometry was subsequently performed

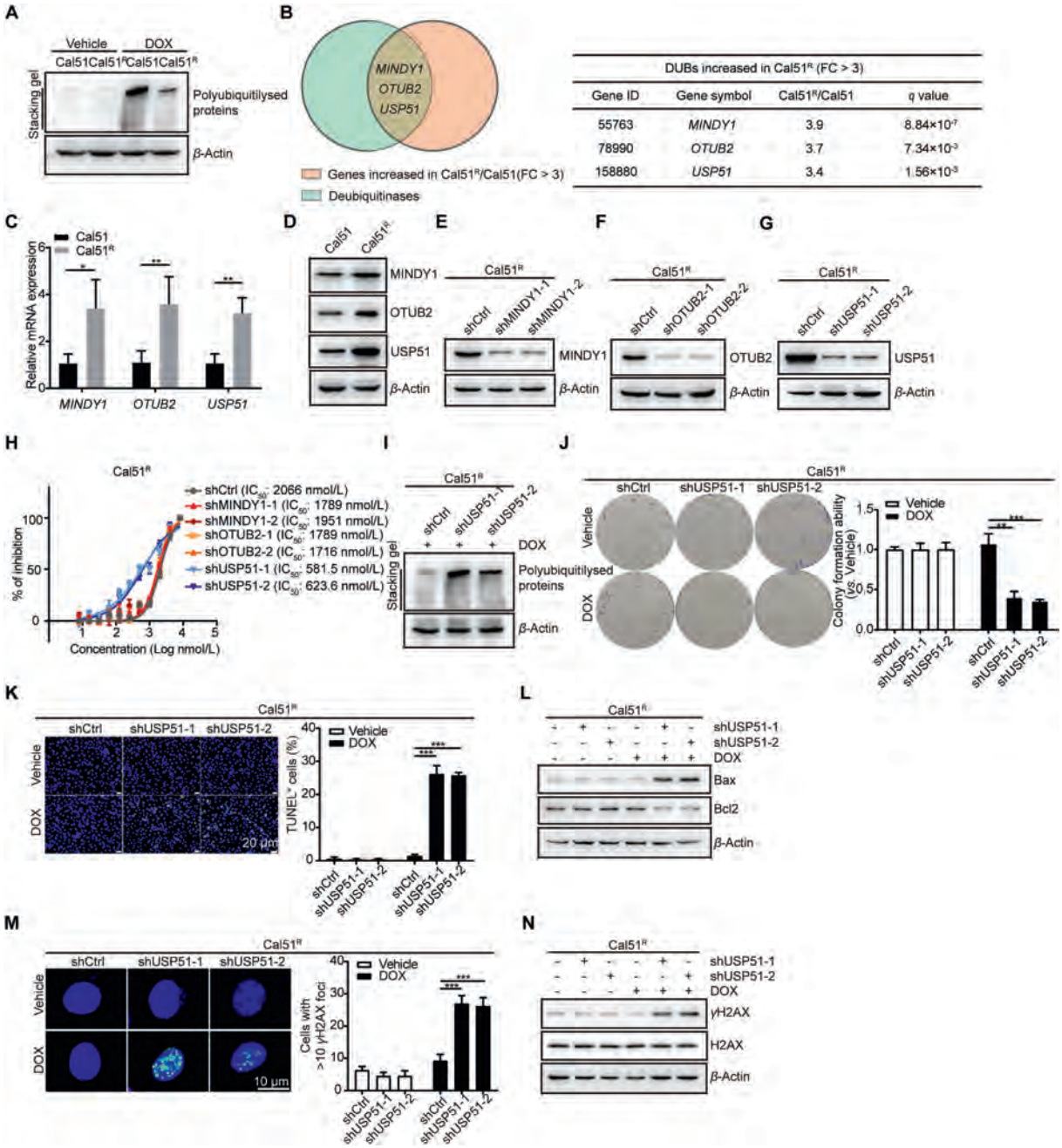

Figure 1 Ectopic ubiquitin-specific protease 51 (USP51) plays a pivotal role in triple-negative breast cancer (TNBC) chemoresistance. (A) Western blotting analysis of polyubiquitinated protein expression in Cal51 and Cal51^R cells. (B−D) RNA sequencing (B), q-PCR (C) and Western blotting (D) of MIU-containing novel DUB family member 1 (MINDY1), OTU domain-containing ubiquitin aldehyde-binding protein 2 (OTUB2) and USP51 expression in Cal51 and Cal51^R cells. (E) Western blotting of MINDY1 expression in MINDY1-knockdown Cal51^R cells. (F) Western blotting of OTUB2 expression in OTUB2-knockdown Cal51^R cells. (G) Western blotting of USP51 expression in USP51-knockdown Cal51^R cells. (H) Cell Counting Kit-8 (CCK-8) assay of Cal51^R cells with knockdown of MINDY1, OTUB2 or USP51. (I) Western blotting analysis of polyubiquitinated protein expression in the USP51-knockdown Cal51^R cells. (J−N) Analyses of colony formation (J), cell apoptosis (K, L) and γH2AX expression (M, N) in USP51-knockdown Cal51^R cells treated with doxorubicin (DOX) (1 μmol/L). $^*P < 0.05$, $^{**}P < 0.01$, $^{***}P < 0.001$; the data in C, J, K and M were assessed *via* unpaired Student's *t*-test. The data are presented as the mean ± SD in (C, H, J, K, M). The data are representative of four (H) or three (C, J, K, M) independent experiments.

for Cal51^R cells (Supporting Information Table S5). As shown in Fig. 3A, eukaryotic orthologous group (KOG) classification analysis demonstrated that cellular proteins interacting with USP51 were involved mainly in posttranslational modification and chaperone processes. Three members of the heat shock protein 70 (HSP70) family, including GRP75, HSPA8, and GRP78, were most significantly enriched. We further validated the physical interactions of USP51 with GRP75 (Fig. 3B), HSPA8 (Fig. 3C)

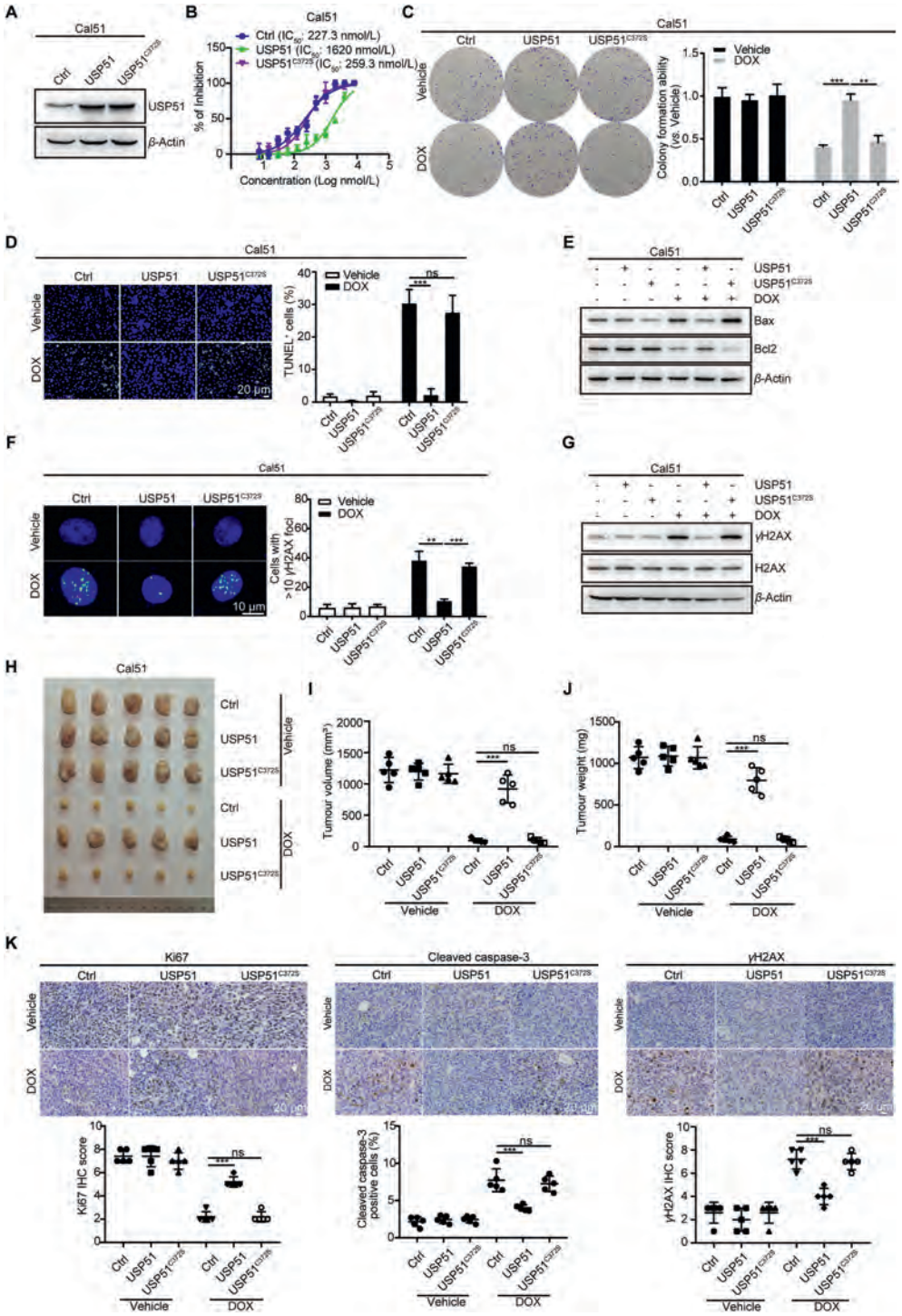

Figure 2 USP51 promotes TNBC chemoresistance *via* its DUB activity. (A) Western blotting of USP51 expression in USP51-expressing Cal51 cells. (B−G) Analyses of cell viability (B), colony formation (C), cell apoptosis (D, E) and γH2AX expression (F, G) in USP51-expressing Cal51 cells treated with DOX (1 μmol/L). (H) Representative image of tumors dissected from xenograft model mice treated with DOX (2 mg/kg). (I, J) Quantification of the volume (I) and weight (J) of tumors derived from the respective xenograft tumors. (K) Immunohistochemical staining of Ki67, cleaved caspase-3 and γH2AX in the respective xenograft tumors. $^{**}P < 0.01$, $^{***}P < 0.001$; ns represents no significant difference; the data in C, D, F and I−K were assessed *via* unpaired Student's *t*-test. The data are presented as the mean ± SD in (B−D, F, I−K). The dots represent individual samples in (I−K). The data are representative of four (B), three (C, D, F) or five (I−K) independent experiments.

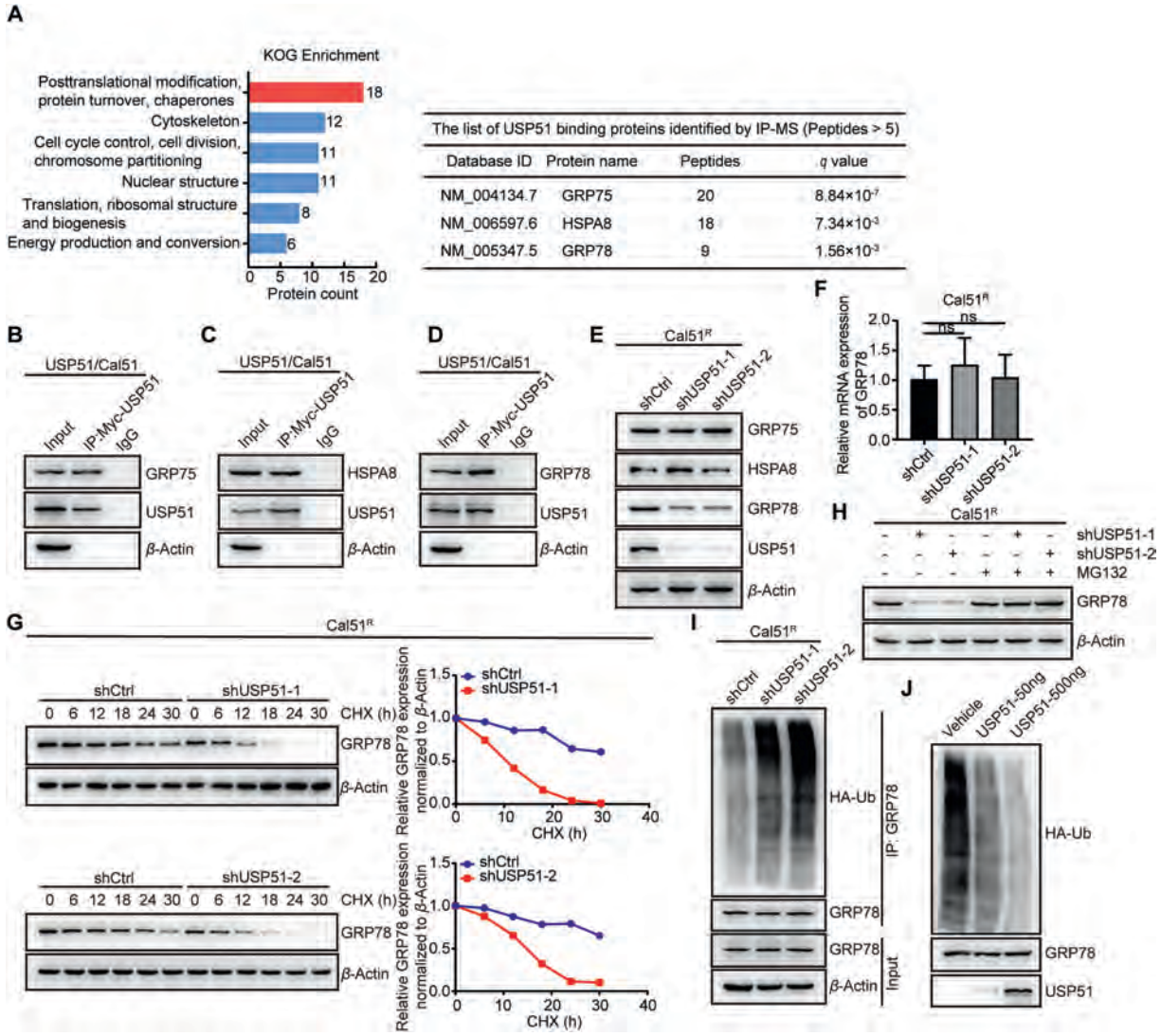

Figure 3 USP51 deubiquitinates and stabilizes 78 kDa glucose-regulated protein (GRP78). (A) Mass spectrum analysis of USP51-binding proteins. (B−D) Co-IP assays of the interaction of USP51 with GRP75 (B), HSPA8 (C) and GRP78 (D) in USP51-expressing Cal51 cells. (E) Western blotting of GRP75, HSPA8, GRP78 and USP51 expression in USP51-knockdown Cal51^R cells. (F) Q-PCR analysis of GRP78 expression in USP51-knockdown Cal51^R cells. (G) Cycloheximide (CHX) (100 μmol/L) pulse-chase analysis of GRP78 in USP51-knockdown Cal51^R cells. (H) Western blotting of GRP78 expression in USP51-knockdown Cal51^R cells treated with MG132 (20 μmol/L). (I) Western blotting analysis of GRP78 ubiquitination in USP51-knockdown Cal51^R cells. (J) *In vitro* deubiquitination assay of GRP78 with purified USP51 protein. ns represents no significant difference. The data in F were assessed *via* unpaired Student's *t*-test. The data in F are presented as the mean ± SD. The data in F are representative of three independent experiments.

and GRP78 (Fig. 3D) in Cal51^R cells. However, Western blotting analysis revealed that USP51 knockdown specifically reduced the protein levels of GRP78, but not those of GRP75 or HSPA8, in Cal51^R cells (Fig. 3E). In addition, we demonstrated that the mRNA level of *GRP78* was barely affected by USP51 depletion (Fig. 3F). Functionally, the CHX pulse-chase assay confirmed the decreased protein stability of GRP78 in shUSP51/Cal51^R cells (Fig. 3G). In line with these findings, the USP51 knockdown-mediated increase in GRP78 content was greatly attenuated by the addition of the proteasome inhibitor MG132 (Fig. 3H). Notably, USP51 depletion markedly increased the level of ubiquitinated GRP78 in Cal51^R cells (Fig. 3I), which was further validated in MDA-MB-231 cells (Supporting Information Fig. S4). Taken together with the results of the deubiquitination assay showing that USP51 decreased the ubiquitination level of GRP78 *in vitro* (Fig. 3J), these results collectively indicate that USP51, as a *bona fide* DUB, plays a pivotal role in targeting the GRP78 protein for deubiquitination and stabilization.

3.4. USP51 deubiquitinates GRP78 at lysine residues K547 and K556

In addition, as shown in Fig. 4A and B, a series of deletion mutants for USP51 (Myc-USP51-N and Myc-USP51-C) and GRP78 (Flag-GRP78-G1, Flag-GRP78-G2, Flag-GRP78-G3, and Flag-GRP78-G4) were generated and expressed in Cal51 cells. Co-IP assays revealed that the deletion variant USP51−N was able to interact with GRP78-G4. These experiments were also validated in MDA-MB-

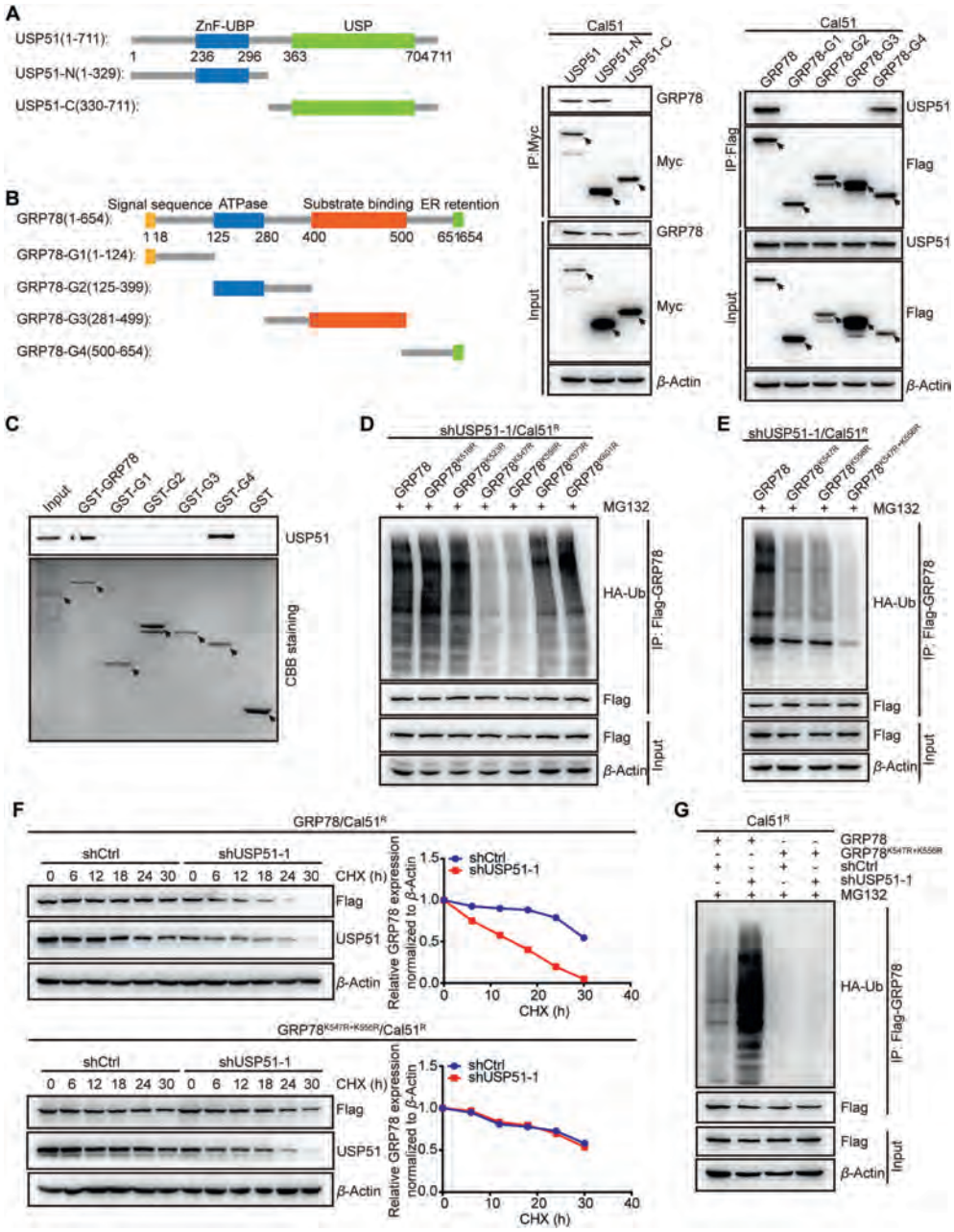

Figure 4 USP51 deubiquitinates GRP78 at lysine residues K547/K556. (A) Co-IP assay of the interaction of GRP78 with USP51 mutants in Cal51 cells. (B) Co-IP assay of the interaction of USP51 with GRP78 mutants in Cal51 cells. (C) *In vitro* binding assay of purified His-USP51 and GST-GRP78-mutant proteins. (D) Western blotting of GRP78 ubiquitination in shUSP51/Cal51^{R} cells overexpressing wild-type or site-directed mutants of GRP78 (K516R-GRP78, K523R-GRP78, K547R-GRP78, K556R-GRP78, K573R-GRP78, and K601R-GRP78). (E) Western blotting of GRP78 ubiquitination in shUSP51/Cal51^{R} cells overexpressing the wild-type GRP78 or the indicated mutants of GRP78 (K547R-GRP78, K556R-GRP78, K547R + K556R-GRP78). (F) CHX (100 μmol/L) pulse-chase analysis of GRP78 in shCtrl/Cal51^{R} or shUSP51/Cal51^{R} cells overexpressing the wild-type or indicated mutant of GRP78 (K547R + K556R-GRP78). (G) Western blotting of GRP78 ubiquitination in shCtrl/Cal51^{R} or shUSP51/Cal51^{R} cells overexpressing the wild-type or indicated mutant of GRP78 (K547R + K556R-GRP78).

231 cells (Supporting Information Fig. S5). Importantly, an *in vitro* binding assay was performed to prove that the purified His-USP51 and GST-GRP78-G4 proteins physically interact under cell-free conditions (Fig. 4C). To further investigate whether USP51 deubiquitinated the lysine residues of GRP78-G4, wild-type GRP78 and individual GRP78 mutants (K516R, K523R, K547R, K556R, K573R, and K601R) were transfected into shUSP51-1/Cal51^{R} cells (Fig. 4D). The results of the ubiquitination assay indicated that the polyubiquitination levels of either K547R or K556R were markedly reduced as compared with the wild-type GRP78; however, this effect was not observed for the K516R, K523R, K573R, and K601R mutants. Notably, simultaneous K547R + K556R mutations completely blocked the polyubiquitination of GRP78 (Fig. 4E), confirming that lysine residues K547 and K556 are major ubiquitination sites on

GRP78. Consistent with these findings, USP51 knockdown strongly reduced the stability and increased the ubiquitination level of the wild-type GRP78 protein; however, this effect was abolished in cells harboring the simultaneous K547R + K556R mutations (Fig. 4F and G). These experiments were also validated in MDA-MB-231^{R} cells, and similar results were obtained (Supporting Information Fig. S6). Collectively, our observations suggest that lysine residues K547 and K556 on the C-terminal region of GRP78 are necessary for deubiquitination and stabilization by USP51 in chemoresistant TNBC cells.

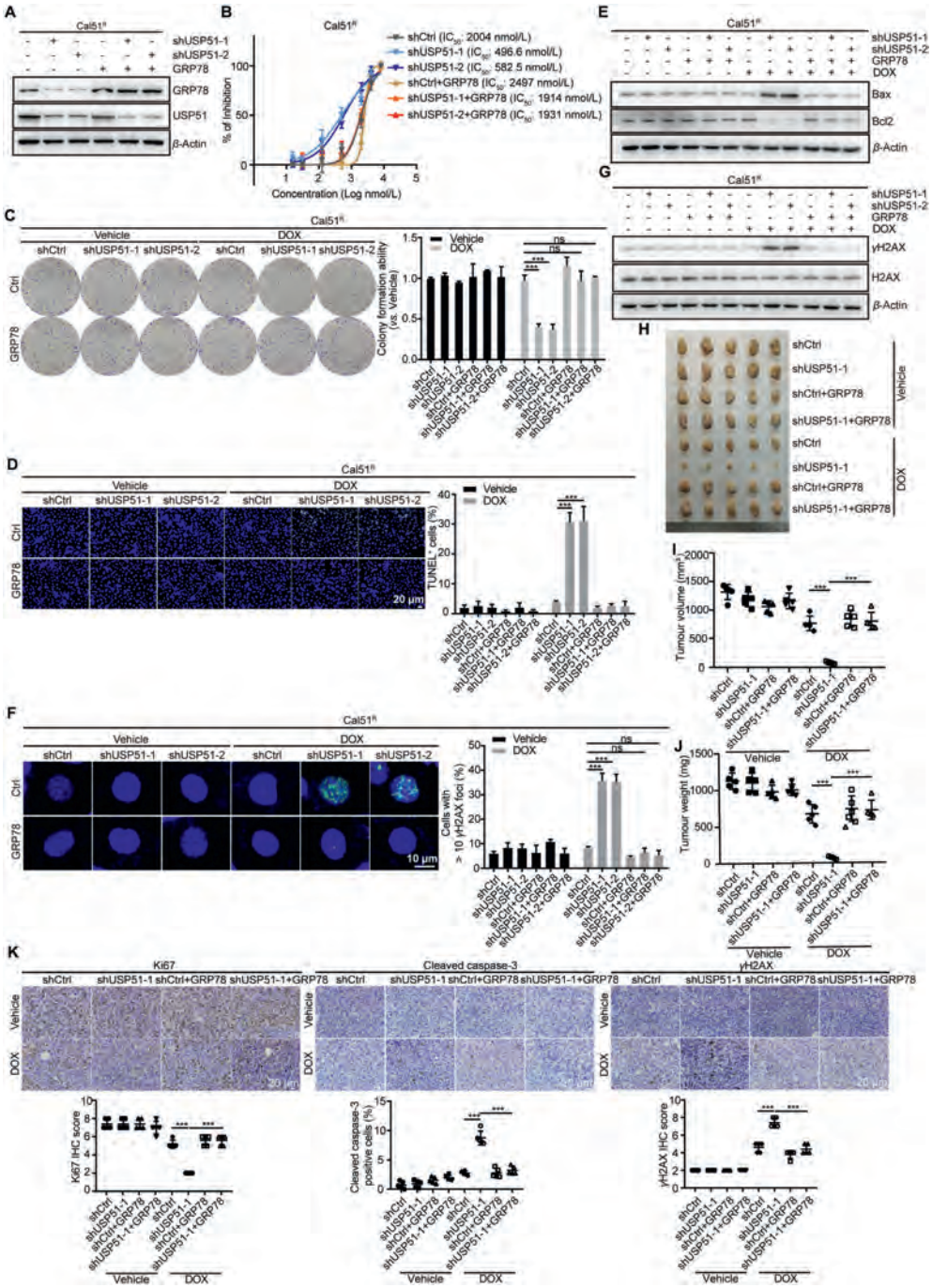

Figure 5 USP51 promotes TNBC chemoresistance by deubiquitinating GRP78. (A) Western blotting of GRP78 and USP51 expression in GRP78-expressing shUSP51/Cal51^{R} cells. (B−G) Analyses of cell viability (B), colony formation (C), cell apoptosis (D, E) and γH2AX expression (F, G) in GRP78-expressing shUSP51/Cal51^{R} cells treated with DOX (1 μmol/L). (H) Representative image of tumors dissected from xenograft model mice treated with DOX (2 mg/kg). (I, J) Quantification of the volume (I) and weight (J) of tumors derived from the respective xenograft tumors. (K) Immunohistochemical staining of Ki67, cleaved caspase-3 and γH2AX in the respective xenograft tumors. ***$P < 0.001$; ns represents no significant difference; the data in C, D, F and I−K were assessed *via* unpaired Student's *t*-test. The data are presented as the mean ± SD in (B−D, F, I−K). The dots represent individual samples in (I−K). The data are representative of four (B), three (C, D, F) or five (I−K) independent experiments.

3.5. USP51 promotes TNBC chemoresistance by deubiquitinating GRP78

Next, we investigated whether ectopic USP51 affects the chemotherapeutic sensitivity of TNBC cells in a GRP78-dependent manner. To do so, the expression of GRP78 was rescued in shUSP51/Cal51^R cells (Fig. 5A). The results of the cell viability (Fig. 5B), colony formation (Fig. 5C), cell apoptosis (Fig. 5D and E), and DNA damage detection (Fig. 5F and G) assays indicated that the sensitivity to DOX was increased in shUSP51/Cal51^R cells, whereas this effect was significantly attenuated in GRP78-expressing cells. We also observed similar results in MDA-MB-231^R cells (Supporting Information Fig. S7). Consistently, using the Nod-SCID xenograft tumor model, we confirmed that USP51 knockdown had a chemosensitizing effect upon DOX treatment, and this effect was strongly attenuated in mice with GRP78-expressing tumors (Fig. 5H–J). Immunohistochemical staining further revealed that the expression of Ki67 was

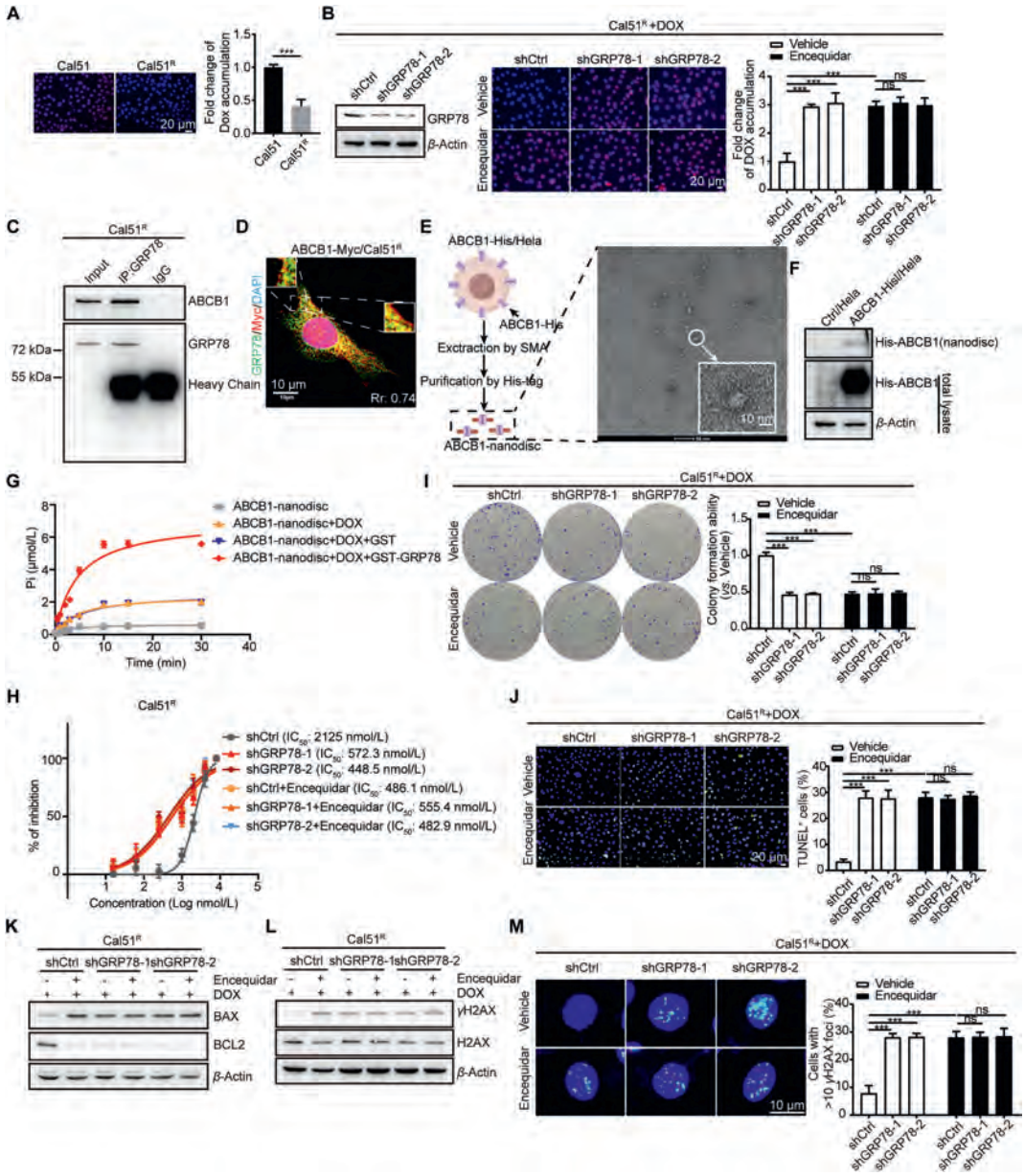

Figure 6 GRP78 promotes TNBC chemoresistance by regulating ATP binding cassette subfamily B member 1 (ABCB1)-mediated DOX efflux. (A) Fluorescence detection of DOX in Cal51 and Cal51^R cells. (B) Western blotting of GRP78 and fluorescence detection of DOX in GRP78-treated Cal51^R cells treated with DOX (1 μmol/L) in the presence or absence of Encequidar (100 nmol/L). (C) Co-IP assay of GRP78 and ABCB1 in Cal51^R cells. (D) Immunofluorescence staining of GRP78 and ABCB1 in ABCB1-Myc/Cal51^R. (E) Analysis of ABCB1 nanodiscs *via* electron microscopy. (F) Western blotting of ABCB1 expression in nanodiscs derived from Ctrl/HeLa and ABCB1/HeLa cells. (G) ATPase activity assay of ABCB1 nanodiscs with purified GST or GST-GRP78 proteins. (H–M) Cell viability (H), colony formation (I), cell apoptosis (J, K) and γH2AX foci formation (L, M) were examined in shGRP78/Cal51^R cells treated with DOX alone or in combination with Encequidar (100 nmol/L). ***$P < 0.001$; ns represents no significant difference; the data in A, B, I, J and M were assessed *via* unpaired Student's *t*-test. The data are presented as the mean ± SD in (A, B, G–J, M). The data are representative of three (A, B, G, I, J, M) or four (H) independent experiments.

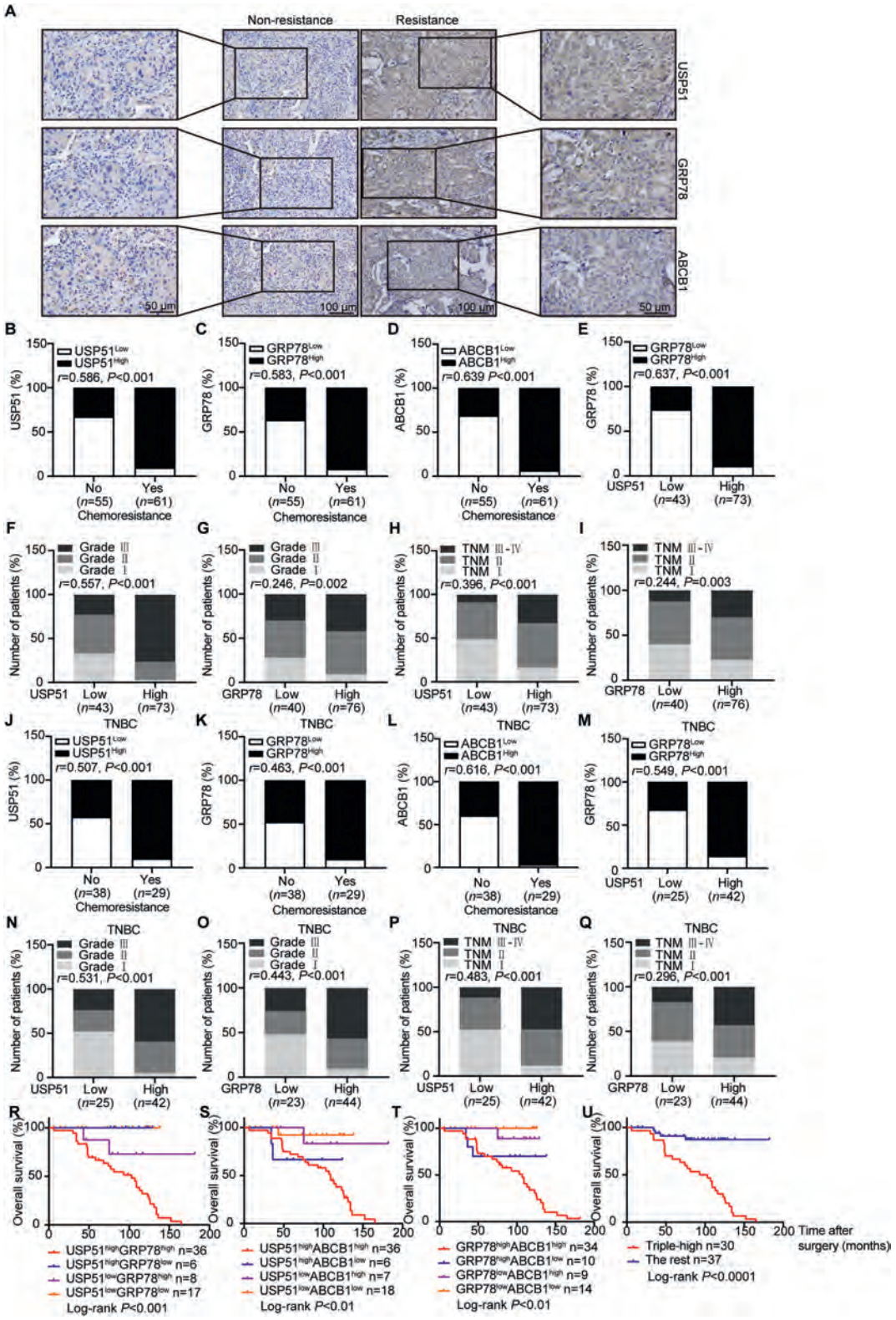

Figure 7 Increased expression of USP51, GRP78 and ABCB1 is correlated with chemoresistance in TNBC. (A) Representative image of immunohistochemical staining of USP51, GRP78 and ABCB1 in serial sections from chemoresistant and nonresistant tumors is shown. (B−D) Direct associations of USP51, GRP78 and ABCB1 expression with chemoresistance were observed in human breast cancer samples. (E) Positive correlation between USP51 and GRP78 expression was observed in human breast cancer samples. (F, G) A positive correlation between the USP51 and GRP78 contents and pathological grade was observed in human breast cancer samples. (H, I) Direct associations between USP51 and GRP78 expression levels and advanced TNM stage were observed in human breast cancer samples. (J−L) Direct associations of USP51, GRP78 and ABCB1 expression with chemoresistance were observed in human TNBC samples. (M) A positive correlation between USP51

reduced but the expression of cleaved caspase-3 and γH2AX was increased in shUSP51/Cal51^R tumors upon DOX treatment, and these effects were suppressed in tumors in which GRP78 expression was restored (Fig. 5K). These results collectively illustrate that ectopic USP51 contributes to TNBC chemoresistance by modulating GRP78 both *in vivo* and *in vitro*.

3.6. GRP78 promotes TNBC chemoresistance via ABCB1-mediated drug efflux

Previous studies have shown that insufficient accumulation of DOX plays a pivotal role in the emergence of chemoresistance in human cancers[42]. In line with these findings, we demonstrated significant suppression of DOX accumulation in Cal51^R cells compared with that in control Cal51 cells (Fig. 6A). Interestingly, specific knockdown of GRP78 abolished this effect to promote DOX accumulation in shGRP78/Cal51^R cells (Fig. 6B). Considering that the membrane-associated protein ATP-binding cassette subfamily B member 1 (ABCB1), a member of the ABC transporter superfamily, functions as the main efflux pump of DOX in chemoresistant TNBC cells[43], we further detected whether GRP78 alters DOX efflux in an ABCB1-dependent manner. Indeed, the results indicated that treatment with Encequidar, which is a specific inhibitor of ABCB1, promoted DOX accumulation in shCtrl/Cal51^R cells; however, this effect was strongly inhibited upon GRP78 depletion (Fig. 6B). Mechanistically, the Co-IP assay results demonstrated that ABCB1 physically interacts with GRP78 in Cal51^R cells (Fig. 6C). In line with these findings, we observed colocalization of GRP78 and ABCB1 on the plasma membrane of ABCB1-expressing Cal51^R cells *via* immunofluorescence staining (Fig. 6D). To further assess whether the interaction with GRP78 affects ABCB1-mediated DOX efflux, we prepared plasma membrane nanodiscs with integrated His-tagged ABCB1 in HeLa cells; they were approximately 10 nm in diameter according to electron microscopy (Fig. 6E). The expression of ABCB1 in the nanodiscs was also confirmed by Western blotting (Fig. 6F). Notably, the *in vitro* ATPase activity assay demonstrated that ABCB1-mediated DOX efflux, as indicated by phosphate ion generation mediated by ATP hydrolysis, was specifically enhanced in the group with the addition of GST-GRP78 compared with the GST control group (Fig. 6G).

Functionally, the results of the cell viability (Fig. 6H), colony formation (Fig. 6I), cell apoptosis (Fig. 6J and K), and DNA damage detection (Fig. 6L and M) assays confirmed that the responsiveness to DOX treatment was markedly increased in shGRP78/Cal51^R cells, whereas these outcomes were abolished by the addition of Encequidar. We also obtained similar results in MDA-MB-231^R cells (Supporting Information Fig. S8), revealing that ectopic GRP78 affects TNBC cell sensitivity to chemotherapy by regulating ABCB1-mediated DOX efflux.

3.7. The expression of USP51, GRP78, and ABCB1 is positively correlated with chemotherapeutic resistance in breast cancer patients

To further validate the relationship between the USP51−GRP78−ABCB1 axis and chemoresistance-related pathological features in breast cancer patients, we performed immunohistochemical staining of USP51, GRP78, and ABCB1 in breast cancer samples from 116 patients treated with anthracycline-based neoadjuvant chemotherapy (Fig. 7A). The samples were divided into two groups on the basis of the Response Evaluation Criteria in Solid Tumors (RECIST). The results demonstrated that the expression of USP51 (Fig. 7B), GRP78 (Fig. 7C), and ABCB1 (Fig. 7D) in chemoresistant tumors was significantly greater than that in sensitive tumors. We also observed a positive correlation between USP51 and GRP78 (Fig. 7E). In addition, we observed increased USP51 and GRP78 levels in high-grade tumors (Fig. 7F and G) and tumors with advanced tumor-node-metastasis (TNM) stages (Fig. 7H and I). Importantly, we validated these results in a subcohort of 67 patients with TNBC (Fig. 7J−Q). Notably, TNBC patients with substantially elevated USP51, GRP78, and ABCB1 expression in tumors presented shorter overall survival than patients with low USP51, GRP78, and ABCB1 expression (Fig. 7R−T). We also confirmed that patients with concomitantly high expression of USP51, GRP78, and ABCB1 in tumors had significantly shorter overall survival than those with other expression patterns (Fig. 7U). Taken together, these data revealed that dysregulation of the USP51/GRP78/ABCB1 axis potentially contributes to the cellular mechanisms that mediate breast cancer chemoresistance and its poor prognosis.

3.8. WCY-4-1 is a potent USP51 inhibitor

In our previous investigation, we discovered that the natural product dihydromyricetin (DHM, $IC_{50} = 0.48 \pm 0.06$ μmol/L) is a USP51 inhibitor through high-throughput screening[39]. DHM is part of a flavonoid class of natural products with some defects in the core structure, which limits its further structural modification; its features include poor water solubility, low oral bioavailability, and rapid metabolism *in vivo*. We thus aimed to screen more suitable, nonnatural core structures for further identification of USP51 inhibitors. To achieve this goal, we analyzed and simulated the plausible conformations of DHM. It was discovered that the natural molecule consists of two conjugated π-moieties (MA and MB) with a dihedral angle of approximately 50° (Fig. 8A), which might represent the "3D shape" of the USP51 protein pocket for binding to DHM. On the basis of these findings, we performed ligand conformation similarity-based screening for a commercially available molecule library containing more than 100,000 compounds, utilizing DHM as the inquiry structure. This investigation led to the identification of several conformational analogs of DHM (Fig. 8B). The USP51 enzyme activities of the compounds with the 50 highest scores were subsequently assessed *in vitro* (Fig. 8C and Supporting Informaiton Table S6). Compound F858-0166 exhibited robust enzymatic inhibition (with a 72.4% inhibition rate at 1 μmol/L and an $IC_{50} = 420$ nmol/L). We further found that the conjugated aromatic system (MA and MB) of F858-0166 was similar to that of DHM (Fig. 8A and D). Additionally, it also extended to a moiety C (MC) component linked with a rotatable −NH− band (Fig. 8D). This discovery indicates a new direction for research on structure optimization and novel structure−activity relationships (SARs). Extensive structural modification and SAR studies on the molecular units

expression and GRP78 expression was observed in human TNBC samples. (N, O) A positive association between USP51 and GRP78 expression levels and pathological grade was observed in human TNBC samples. (P, Q) Direct associations between USP51 and GRP78 contents and advanced TNM stage were observed in human TNBC samples. (R−U) Kaplan−Meier curves of overall survival in TNBC patients with high or low expression of USP51, GRP78 and ABCB1 in their breast tumors. The data in B−U were assessed *via* Spearman's rank correction test.

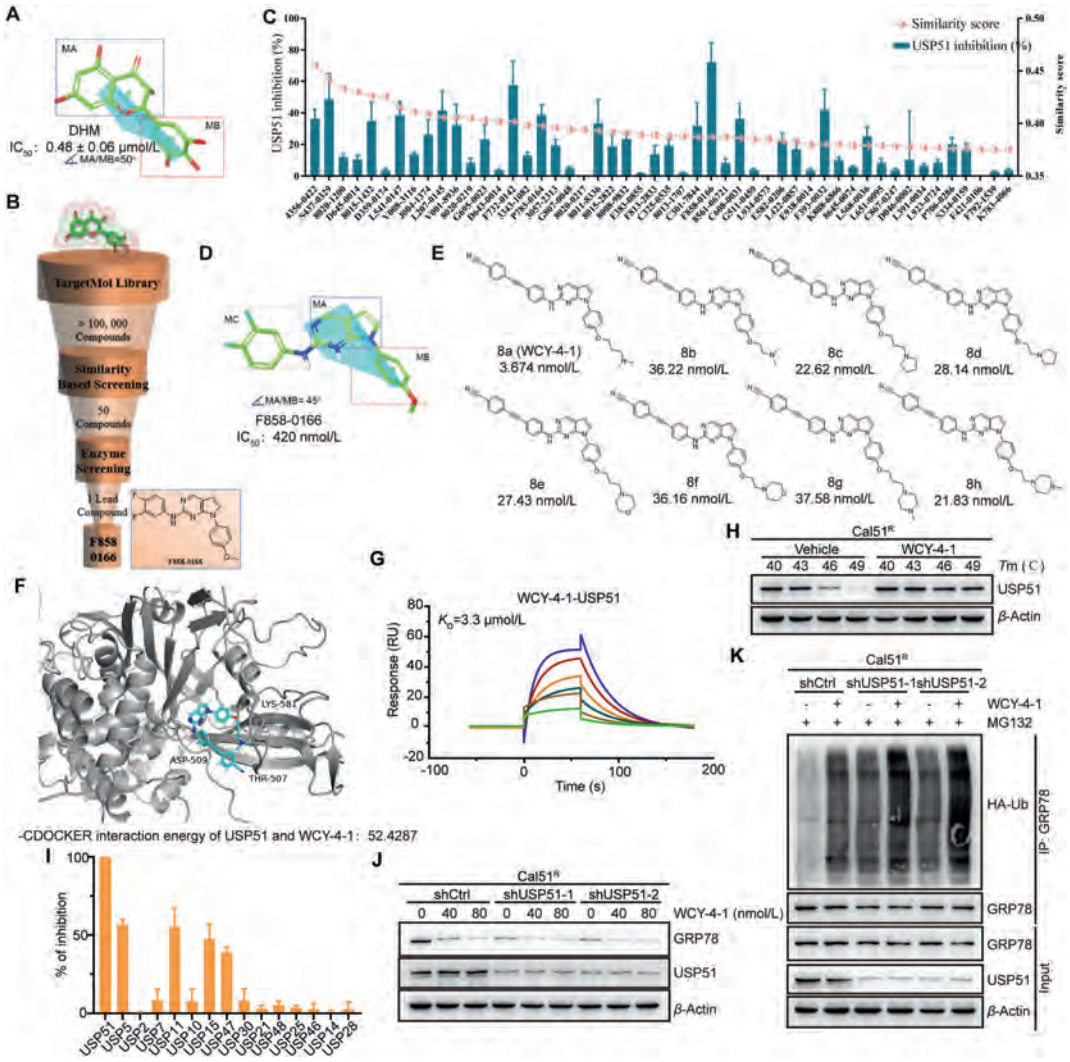

Figure 8 WCY-4-1 was identified as a potent USP51 inhibitor. (A) Conformation analysis of dihydromyricetin. (B) Flow chart of the conformation-similarity-based virtual screen. (C) Enzyme activity test for the compounds with the 50 highest scores. (D) Conformation analysis of F858-0166. (E) Structures of synthetic analogs derived from F858-0166. (F) Binding affinity analysis between the catalytic domain of USP51 and WCY-4-1 *via* computational molecular dynamic simulation. (G) K_d values between USP51 and WCY-4-1 according to the SPR binding assay. (H) Cellular thermal shift assay for USP51 interaction with WCY-4-1 in Cal51^R cells. (I) The inhibitory effect of WCY-4-1 on the activity of USP family members was determined *via* a Ub-AMC assay. (J) Western blotting of GRP78 and USP51 expression in USP51-knockdown Cal51^R cells treated with WCY-4-1. (K) Western blotting of GRP78 ubiquitination in USP51-knockdown Cal51^R cells treated with WCY-4-1 (80 nmol/L). The data are presented as the mean ± SD in (C, I). C, I are representative of three independent experiments.

MA, MB, and MC were then performed according to the classic group replacement strategy. Our findings indicated that simultaneously elongating the hydrophobic MC and introducing appropriate hydrophilic groups at the ortho-position of the π-structure MB may significantly improve the inhibitory activity against USP51. Compound 8a, named WCY-4-1, was discovered to be the most potent USP51 inhibitor (IC_{50} value of 3.674 nmol/L, Fig. 8E and Supporting Informaiton Table S7) and was selected as the lead compound for further validation. In addition, the results of the computational molecular dynamics simulation demonstrated that WCY-4-1 could bind to the catalytic domain of USP51 (Fig. 8F). We also performed a surface plasmon resonance (SPR) binding assay to validate the strong binding affinity between WCY-4-1 and USP51 (Fig. 8G). In line with these findings, the results of the thermal shift assay revealed that WCY-4-1 treatment significantly increased the stability of the USP51 protein in both Cal51^R (Fig. 8H) and MDA-MB-231^R cells (Supporting Information Fig. S9), indicating that WCY-4-1 might directly target USP51. Importantly, we determined that WCY-4-1 specifically decreased the activity of USP51 among its family members *via* an *in vitro* deubiquitinase activity assay (Fig. 8I).

Moreover, as shown in Fig. 8J, treatment with WCY-4-1 significantly downregulated the expression of GRP78 in Cal51^R cells in a dose-dependent manner; however, this effect was strongly inhibited by USP51 depletion. Consistently, the results of the ubiquitination assays confirmed that USP51 deubiquitinase inhibition by treatment with WCY-4-1 led to increased polyubiquitination of the GRP78 protein in Cal51^R cells, which was significantly impaired in response to USP51 depletion (Fig. 8K). In contrast, wild-type USP51 and its catalytically inactive mutant USP51^{C372S} were introduced into Cal51 cells, which were subsequently treated with WCY-4-1 (Supporting Information

Fig. S10A). Our Western blotting results revealed that the expression of GRP78 was markedly upregulated in USP51/Cal51 cells, and this effect was further weakened by WCY-4-1 treatment in a dose-dependent manner. In line with these findings, the results of the ubiquitination assay revealed that USP51 deubiquitinase inhibition by treatment with WCY-4-1 led to increased polyubiquitination of the GRP78 protein in USP51/Cal51 cells (Fig. S10B). Notably, these outcomes were not observed in cells with the USP51^{C372S} mutant, revealing that WCY-4-1 exert its biological function through a USP51-dependent mechanism. We also performed these experiments in MDA-MB-231 cells and obtained similar results (Supporting Information Fig. S11).

3.9. WCY-4-1 treatment confers chemosensitivity in TNBC

Consequently, we investigated whether WCY-4-1 can alter the chemoresistance-related properties of TNBC cells. Indeed, treatment with WCY-4-1 increased DOX-induced cell proliferation arrest (Fig. 9A and B), cell apoptosis (Fig. 9C and D), and the DDR (Fig. 9E and F) in Cal51^{R} cells, while these effects were markedly inhibited by USP51 interference. On the other hand, wild-type USP51-induced chemoresistance phenotypes were attenuated by the addition of WCY-4-1 to Cal51 cells (Supporting Information Fig. S12). However, these outcomes were not observed for the USP51^{C372S} mutant, demonstrating that WCY-4-1 confers responsiveness to chemotherapeutic treatment in a

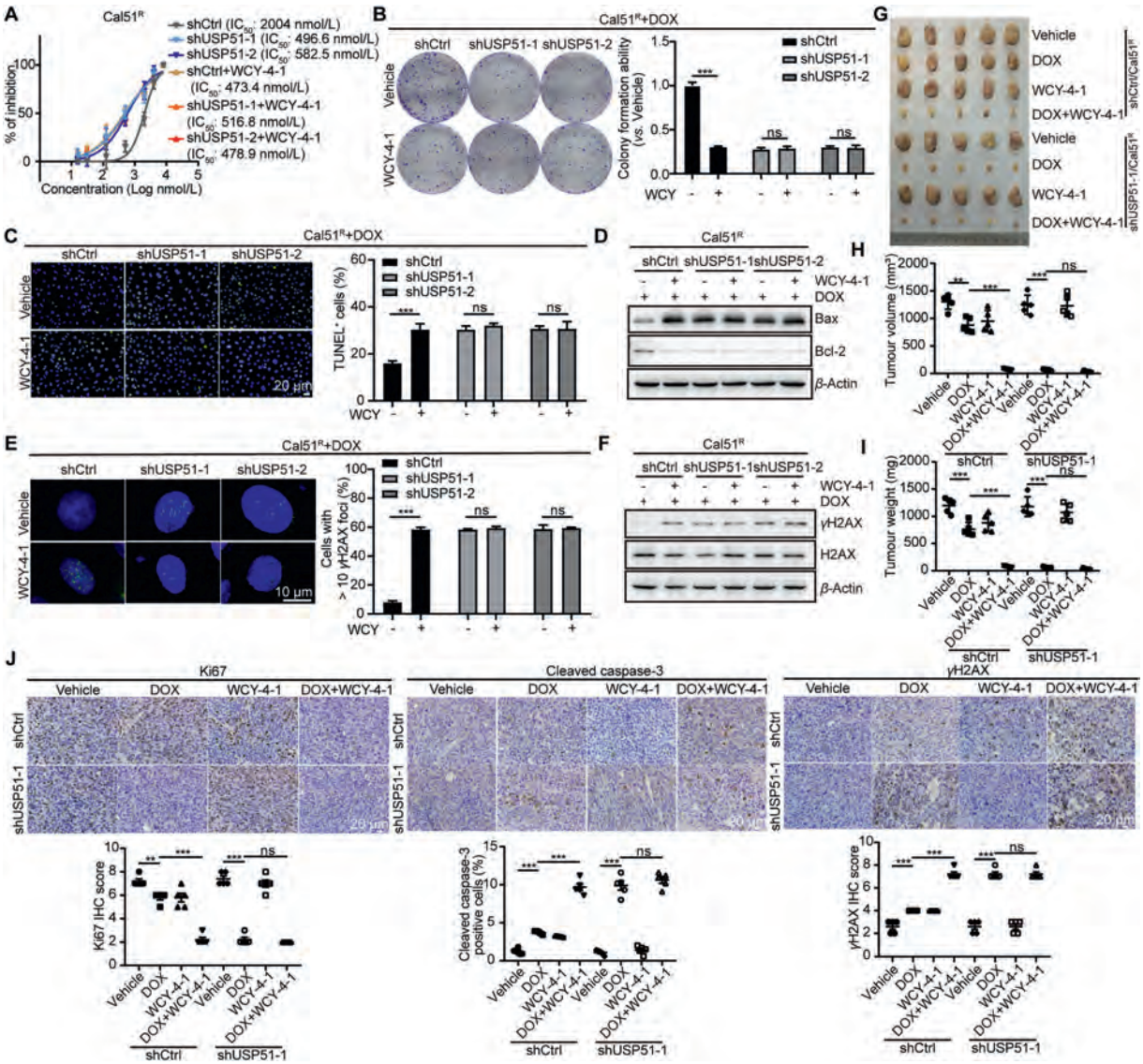

Figure 9 WCY-4-1 treatment confers DOX sensitivity in TNBC. (A−F) Cell viability (A), colony formation (B), cell apoptosis (C, D) and γH2AX expression (E, F) were assessed in shUSP51/Cal51^{R} cells treated with DOX alone or in combination with WCY-4-1 (80 nmol/L). (G) Representative images of tumors dissected from xenograft model mice treated with DOX (2 mg/kg) and/or WCY-4-1 (2 mg/kg). (H, I) Quantification of the volume (H) and weight (I) of tumors derived from the respective xenograft model groups. (J) Immunohistochemical staining of Ki67, cleaved caspase-3 and γH2AX in the respective xenograft tumors. $^{**}P < 0.01$, $^{***}P < 0.001$; ns represents no significant difference; the data in B, C, E and H−J were assessed *via* unpaired Student's *t*-test. The data are presented as the mean ± SD in (A−C, E, H−J). The dots represent individual samples in (H−J). The data are representative of four (A), three (B, C, E) or five (H−J) independent experiments.

USP51-dependent manner in TNBC cells. We also validated the experiments in MDA-MB-231 cells and obtained similar results (Supporting Information Figs. S13 and S14).

Importantly, to explore whether WCY-4-1 treatment can suppress the chemoresistance phenotypes of TNBC cells *in vivo*, shCtrl/Cal51^{R} and shUSP51/Cal51^{R} cells were subcutaneously injected into Nod-SCID mice to establish xenograft tumor models, followed by treatment with DOX alone or combined with WCY-4-1 (Fig. 9G). The results showed that the addition of WCY-4-1 effectively promoted cell sensitivity to DOX in mice bearing shCtrl/Cal51^{R} tumors, as evidenced by a reduction in tumor volume (Fig. 9H) and weight (Fig. 9I) of approximately 80%. However, these effects were completely abolished in shUSP51/Cal51^{R} tumors. Immunohistochemical staining revealed a significant reduction in Ki67 expression but an increase in cleaved caspase-3 and γH2AX expression in shCtrl/Cal51^{R} tumors treated with both DOX and WCY-4-1, whereas these effects were not as evident in shUSP51/Cal51^{R} tumors (Fig. 9J). No obvious undesirable side effects, including reduced body weight (Supporting Information Fig. S15A) or toxic pathological alterations, occurred in the heart, liver, spleen, lung, or kidney (Fig. S15B). Overall, these results indicate that treatment with WCY-4-1 can suppress the chemoresistance phenotypes of TNBC cells and further increase the efficacy of chemotherapy.

4. Discussion

A growing amount of evidence indicates that USP51, a novel DUB that functions in UPS-mediated protein degradation, is involved in the regulation of chemotherapeutic resistance in cancer. Hence, identifying the molecular mechanism that contributes to USP51-triggered chemoresistance may lead to the development of improved antineoplastic strategies. On the basis of our findings, we propose that the intrinsic role of USP51 in chemoresistant TNBC cells is dependent on its DUB activity. Mechanistically, we identified USP51 as a *bona fide* deubiquitinase that marks GRP78 for deubiquitination and stabilization *in vitro* and *in vivo*, eventually promoting ABCB1-mediated chemotherapeutic drug efflux in TNBC cells. Notably, specific inhibition of USP51 markedly sensitized TNBC cells to chemotherapy by impairing GRP78/ABCB1 activity, which provides a feasible solution for future therapeutic interventions for advanced breast cancer (Fig. 10).

Several studies have indicated that elevated USP51 levels are strongly associated with poor outcomes for patients with cancer[33], which corroborates our current findings that high USP51 expression is associated with high tumor grade and advanced TNM stage in breast cancer patients. Notably, our data also suggested that patients who had tumors with high USP51 expression were less likely to benefit from genotoxic drug-based neoadjuvant chemotherapy than those who had tumors with low USP51 expression. Indeed, it was recently reported that ectopic expression of USP51 is associated with chemoresistance phenotypes, such as an impaired DDR, in certain cancer cells[32,33,44]. For example, dysregulation of USP51 activity is clearly observed upon ubiquitination of histone H2A at Lys13,15 (H2AK13,15ub) and thus prevents the recruitment of DNA repair proteins, such as BRCA1 and 53BP1, to damaged chromatin in response to genotoxic drug treatment, which eventually blocks DNA repair *via* both the homologous recombination (HR) and nonhomologous end joining (NHEJ) pathways[32,37]. Here, we further proposed an alternative mechanism for USP51-triggered acquisition of chemotherapeutic resistance by decreasing DOX accumulation in TNBC cells. During this process, USP51, an original deubiquitinase, marks the chaperone protein GRP78 for deubiquitination and stabilization, which consequently activates the efflux transporter ABCB1 to alleviate DNA damage by decreasing DOX accumulation. This new function of USP51 may be inconsistent with the current knowledge that cancer cells are commonly associated with genome instability and that many oncogenes promote, rather than maintain, genome instability[45]. However, a certain level of genome integrity is needed for cancer cells to continue proliferating. The ability of USP51 to promote the DDR is especially important for cancer cell survival and proliferation under conditions of massive DNA damage induced by chemotherapeutic agents and thus serves as a source of cancer-promoting mutations.

Consistent with our findings that GRP78 knockdown led to significantly increased cell sensitivity to DOX in Cal51^{R} cells, recent studies have revealed a positive correlation between

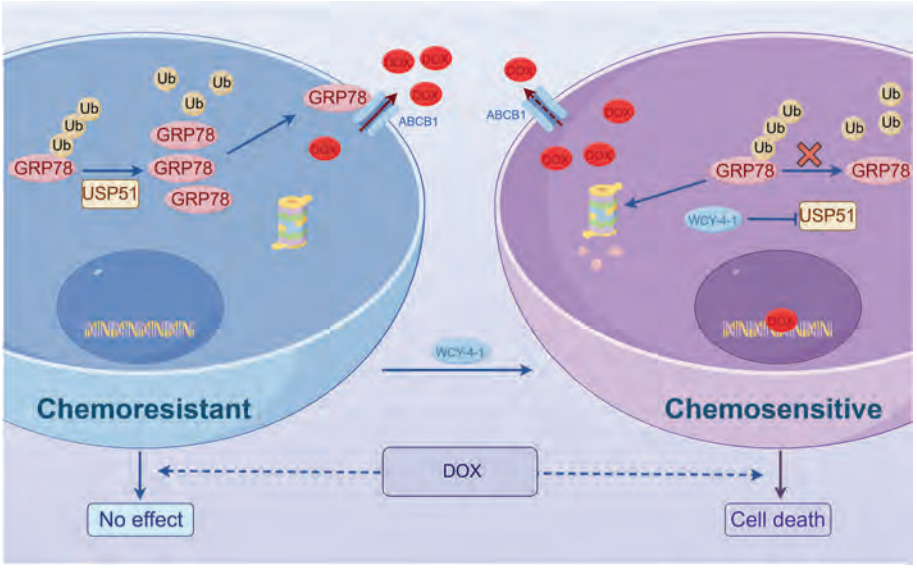

Figure 10 Working model concerning the mechanism of the USP51/GRP78/ABCB1 network in TNBC chemoresistance.

elevated expression of GRP78, chemoresistance, and especially poor prognosis in TNBC[35]. At the molecular level, GRP78 originally functions as an endoplasmic reticulum (ER)-resident chaperone and thus contributes to chemoresistance through its role in maintaining ER homeostasis[46]. For example, GRP78 inhibits ATF4/RET complex formation by binding to RET, thereby stabilizing RET and promoting resistance to the proteasome inhibitor bortezomib in osteosarcoma[47]. Aberrant expression of GRP78 has also been found to be associated with decreased mTOR phosphorylation in gastric cancer, which subsequently intensifies chemotherapeutic resistance by triggering autophagy[48]. In addition, an increasing body of evidence has revealed that, under stress conditions, GRP78 can localize to the cell membrane in association with certain membrane proteins, functioning as a crucial factor in resistance to various targeted therapies[49]. In pancreatic cancer, cell surface GRP78 forms complexes with CRR9 and PI3Kα, activates the PI3K−AKT signaling pathway, and consequently promotes resistance to chemotherapy[50]. Additionally, cisplatin can induce the aggregation of GRP78 on the cell membrane, where it binds to another molecular chaperone, MTJ1/HTJ1, thereby activating the AKT signaling pathway and promoting chemotherapeutic resistance in lung cancer[51]. Here, we found that ectopic USP51 stabilized the GRP78 protein and triggered its cell surface colocalization with ABCB1 in TNBC cells, ultimately promoting ABCB1-mediated drug efflux and the development of chemotherapy resistance. These data collectively suggest that the USP51/GRP78/ABCB1 network contributes to malignant progression and chemotherapeutic resistance in TNBC and may serve as a therapeutic target for cancer management. Given that ABCB1 plays a role in the response to multiple chemotherapeutics, we speculated that the USP51−GRP78−ABCB1 axis may also contribute to resistance to other chemotherapeutic drugs, including vinca alkaloids, antimetabolites and signaling pathway inhibitors such as galunisertib, an inhibitor of the TGF-β signaling pathway[52,53]. Future studies should explore whether the USP51−GRP78−ABCB1 axis regulates resistance to other therapeutic agents, thus expanding our understanding of its alternative role in chemoresistance.

Indeed, the pivotal role of USP51 in tumor development and treatment underscores the importance of developing effective inhibitors specifically targeting USP51[39]. In this study, WCY-4-1, a small molecule inhibitor of USP51, was identified through high-throughput screening. This compound demonstrated a potent inhibitory effect against USP51 *in vitro* (IC_{50} = 3.674 nmol/L) and good *in vivo* tolerance. WCY-4-1 cannot only block DOX efflux caused *via* the USP51−GRP78−ABCB1 axis but also impair USP51-mediated deubiquitination and the stability of histones and DDR-related proteins to inhibit the self-repair of TNBC cells[32,37,44]. Although AlphaFold was used to predict the structure of USP51, the lack of a cocrystal structure of USP51 with WCY-4-1 prevented us from determining the binding site of WCY-4-1 and increasing its selectivity due to the high flexibility of the USP51 protein. Therefore, further identification of the cocrystal structure of USP51 with WCY-4-1 will be beneficial for the optimization of specific small-molecule inhibitors of USP51.

5. Conclusions

In summary, we demonstrated an alternative mechanism—USP51−GRP78−ABCB1 axis regulates TNBC chemoresistance by decreasing the accumulation of chemotherapeutic drugs, such as DOX, in cancer cells. Importantly, we identified the potent USP51 inhibitor WCY-4-1 as a drug candidate and identified a new therapeutic strategy to overcome chemoresistance in TNBC, which merits further validation.

Acknowledgments

This work was supported by grants from the International Science and Technology Cooperation Project of China (No. 2022YFE0133300) and the National Natural Science Foundation of China (No. 82472870 and No. 82172801).

Author contributions

Yang Ou: Writing − original draft, Visualization, Validation, Project administration, Methodology, Investigation, Formal analysis, Data curation, Conceptualization. Kun Zhang: Validation, Resources, Methodology. Qiuying Shuai: Methodology, Investigation. Chenyang Wang: Resources, Methodology. Huayu Hu: Visualization, Resources, Methodology. Lixia Cao: Visualization, Validation. Chunchun Qi: Visualization. Min Guo: Visualization, Methodology. Zhaoxian Li: Visualization, Methodology. Jie Shi: Visualization, Methodology. Yuxin Liu: Visualization. Siyu Zuo: Visualization. Xiao Chen: Visualization. Yanjing Wang: Visualization. Mengdan Feng: Visualization. Hang Wang: Visualization. Peiqing Sun: Writing − review & editing, Supervision. Yi Shi: Writing − review & editing, Visualization, Supervision, Resources, Conceptualization. Guang Yang: Writing − review & editing, Supervision, Resources, Conceptualization. Shuang Yang: Writing − review & editing, Supervision, Resources, Funding acquisition, Conceptualization.

Conflicts of interest

The authors declare no conflicts of interest.

Appendix A. Supporting information

Supporting information to this article can be found online at https://doi.org/10.1016/j.apsb.2025.03.004.

References

1. Loibl S, Poortmans P, Morrow M, Denkert C, Curigliano G. Breast cancer. *Lancet* 2021;**397**:1750−69.
2. Denkert C, Liedtke C, Tutt A, von Minckwitz G. Molecular alterations in triple-negative breast cancer-the road to new treatment strategies. *Lancet* 2017;**389**:2430−42.
3. Liao L, Zhang YL, Deng L, Chen C, Ma XY, Andriani L, et al. Protein phosphatase 1 subunit PPP1R14B stabilizes STMN1 to promote progression and paclitaxel resistance in triple-negative breast cancer. *Cancer Res* 2023;**83**:471−84.
4. Leon-Ferre RA, Goetz MP. Advances in systemic therapies for triple negative breast cancer. *BMJ* 2023;**381**:e071674.
5. Korde LA, Somerfield MR, Carey LA, Crews JR, Denduluri N, Hwang ES, et al. Neoadjuvant chemotherapy, endocrine therapy, and targeted therapy for breast cancer: ASCO guideline. *J Clin Oncol* 2021;**39**:1485−505.
6. Gao F, Wu Y, Wang R, Yao Y, Liu Y, Fan L, et al. Precise nanosystem-based drug delivery and synergistic therapy against androgen receptor-positive triple-negative breast cancer. *Acta Pharm Sin B* 2024;**14**:2685−97.

7. Kim C, Gao R, Sei E, Brandt R, Hartman J, Hatschek T, et al. Chemoresistance evolution in triple-negative breast cancer delineated by single-cell sequencing. *Cell* 2018;**173**:879−93.e13.
8. Gomez-Miragaya J, Diaz-Navarro A, Tonda R, Beltran S, Palomero L, Palafox M, et al. Chromosome 12p amplification in triple-negative/BRCA1-mutated breast cancer associates with emergence of docetaxel resistance and carboplatin sensitivity. *Cancer Res* 2019;**79**: 4258−70.
9. Xiong Z, Yang L, Li N, Fu J, Liu P, Sun P, et al. DAB2IP attenuates chemoresistance of triple-negative breast cancer through sequestration of RAC1 to prevent beta-catenin nuclear accumulation. *Clin Transl Med* 2022;**12**:e1133.
10. Yang K, Xu L, Xu Y, Shen Q, Qin T, Yu Y, et al. Nanoparticles (NPs)-mediated lncBCMA silencing to promote eEF1A1 ubiquitination and suppress breast cancer growth and metastasis. *Acta Pharm Sin B* 2023; **13**:3489−502.
11. Liang Y, Min D, Fan H, Liu K, Tu J, He X, et al. Discovery of a first-in-class ANXA3 degrader for the treatment of triple-negative breast cancer. *Acta Pharm Sin B* 2023;**13**:1686−98.
12. He J, Lee HJ, Saha S, Ruan D, Guo H, Chan CH. Inhibition of USP2 eliminates cancer stem cells and enhances TNBC responsiveness to chemotherapy. *Cell Death Dis* 2019;**10**:285.
13. Wang X, Chen T, Li C, Li W, Zhou X, Li Y, et al. CircRNA−CREIT inhibits stress granule assembly and overcomes doxorubicin resistance in TNBC by destabilizing PKR. *J Hematol Oncol* 2022;**15**:122.
14. Han D, Wang L, Jiang S, Yang Q. The ubiquitin−proteasome system in breast cancer. *Trends Mol Med* 2023;**29**:599−621.
15. Ciechanover A. The unravelling of the ubiquitin system. *Nat Rev Mol Cell Biol* 2015;**16**:322−4.
16. Jin J, Tao Z, Cao J, Li T, Hu X. DNA damage response inhibitors: an avenue for TNBC treatment. *Biochim Biophys Acta Rev Cancer* 2021; **1875**:188521.
17. Tutt A, Tovey H, Cheang MCU, Kernaghan S, Kilburn L, Gazinska P, et al. Carboplatin in BRCA1/2-mutated and triple-negative breast cancer BRCAness subgroups: the TNT trial. *Nat Med* 2018;**24**: 628−37.
18. Wang Z, Zhang H, Liu J, Cheruiyot A, Lee JH, Ordog T, et al. USP51 deubiquitylates H2AK13,15ub and regulates DNA damage response. *Genes Dev* 2016;**30**:946−59.
19. Mattiroli F, Penengo L. Histone ubiquitination: an integrative signaling platform in genome stability. *Trends Genet* 2021;**37**:566−81.
20. Liu R, Yang G, Bao M, Zhou Z, Mao X, Liu W, et al. STAMBPL1 promotes breast cancer cell resistance to cisplatin partially by stabilizing MKP-1 expression. *Oncogene* 2022;**41**:2265−74.
21. Yu M, Liu K, Mao Z, Luo J, Gu W, Zhao W. USP11 is a negative regulator to gammaH2AX ubiquitylation by RNF8/RNF168. *J Biol Chem* 2016;**291**:959−67.
22. Chang L, Shen L, Zhou H, Gao J, Pan H, Zheng L, et al. ITCH nuclear translocation and H1.2 polyubiquitination negatively regulate the DNA damage response. *Nucleic Acids Res* 2019;**47**:824−42.
23. Hashemi M, Arani HZ, Orouei S, Fallah S, Ghorbani A, Khaledabadi M, et al. EMT mechanism in breast cancer metastasis and drug resistance: revisiting molecular interactions and biological functions. *Biomed Pharmacother* 2022;**155**:113774.
24. Lin Y, Wang Y, Shi Q, Yu Q, Liu C, Feng J, et al. Stabilization of the transcription factors slug and twist by the deubiquitinase dub3 is a key requirement for tumor metastasis. *Oncotarget* 2017;**8**:75127−40.
25. Wu Y, Wang Y, Lin Y, Liu Y, Wang Y, Jia J, et al. Dub3 inhibition suppresses breast cancer invasion and metastasis by promoting Snail1 degradation. *Nat Commun* 2017;**8**:14228.
26. Yu Q, Zhou BP, Wu Y. The regulation of snail: on the ubiquitin edge. *Cancer Cell Microenviron* 2017;**4**:e1567.
27. Wang H, Yu Y, Jiang Z, Cao WM, Wang Z, Dou J, et al. Next-generation proteasome inhibitor MLN9708 sensitizes breast cancer cells to doxorubicin-induced apoptosis. *Sci Rep* 2016;**6**:26456.
28. Sannino S, Brodsky JL. Targeting protein quality control pathways in breast cancer. *BMC Biol* 2017;**15**:109.
29. Zhang L, Wu M, Su R, Zhang D, Yang G. The efficacy and mechanism of proteasome inhibitors in solid tumor treatment. *Recent Pat Anticancer Drug Discov* 2022;**17**:268−83.
30. Harrigan JA, Jacq X, Martin NM, Jackson SP. Deubiquitylating enzymes and drug discovery: emerging opportunities. *Nat Rev Drug Discov* 2018;**17**:57−78.
31. Sun T, Liu Z, Yang Q. The role of ubiquitination and deubiquitination in cancer metabolism. *Mol Cancer* 2020;**19**:146.
32. Atanassov BS, Mohan RD, Lan X, Kuang X, Lu Y, Lin K, et al. ATXN7L3 and ENY2 coordinate activity of multiple H2B deubiquitinases important for cellular proliferation and tumor growth. *Mol Cell* 2016;**62**:558−71.
33. Hang Q, Zeng L, Wang L, Nie L, Yao F, Teng H, et al. Non-canonical function of DGCR8 in DNA double-strand break repair signaling and tumor radioresistance. *Nat Commun* 2021;**12**:4033.
34. Zhou Z, Zhang P, Hu X, Kim J, Yao F, Xiao Z, et al. USP51 promotes deubiquitination and stabilization of ZEB1. *Am J Cancer Res* 2017;**7**: 2020−31.
35. Zhang Z, Li J, Ou Y, Yang G, Deng K, Wang Q, et al. CDK4/6 inhibition blocks cancer metastasis through a USP51−ZEB1-dependent deubiquitination mechanism. *Signal Transduct Target Ther* 2020;**5**:25.
36. Zhou F, Du C, Xu D, Lu J, Zhou L, Wu C, et al. Knockdown of ubiquitin-specific protease 51 attenuates cisplatin resistance in lung cancer through ubiquitination of zinc-finger E-box binding homeobox 1. *Mol Med Rep* 2020;**22**:1382−90.
37. Walser F, Mulder MPC, Bragantini B, Burger S, Gubser T, Gatti M, et al. Ubiquitin phosphorylation at Thr12 modulates the dna damage response. *Mol Cell* 2020;**80**:423−436.e9.
38. Zhou F, Lu J, Jin W, Li Z, Xu D, Gu L. The role of USP51 in attenuating chemosensitivity of lung cancer cells to cisplatin by regulating DNA damage response. *Biotechnol Appl Biochem* 2023;**70**:634−44.
39. Li J, Xiao X, Ou Y, Cao L, Guo M, Qi C, et al. USP51/PD-L1/ITGB1-deployed juxtacrine interaction plays a cell-intrinsic role in promoting chemoresistant phenotypes in non-small cell lung cancer. *Cancer Commun (Lond)* 2023;**43**:765−87.
40. Liu YJ, Zeng SH, Zhang W, Li JP, Yin Y, Zhuang YW, et al. USP51/ZEB1/ACTA2 axis promotes mesenchymal phenotype in gastric cancer and is associated with low cohesion characteristics. *Pharmacol Res* 2023;**188**:106644.
41. Chang A, Liu L, Ashby JM, Wu D, Chen Y, O'Neill SS, et al. Recruitment of KMT2C/MLL3 to DNA damage sites mediates DNA damage responses and regulates PARP inhibitor sensitivity in cancer. *Cancer Res* 2021;**81**:3358−73.
42. Belisario DC, Akman M, Godel M, Campani V, Patrizio MP, Scotti L, et al. ABCA1/ABCB1 ratio determines chemo- and immune-sensitivity in human osteosarcoma. *Cells* 2020;**9**:647.
43. Ashrafizaveh S, Ashrafizadeh M, Zarrabi A, Husmandi K, Zabolian A, Shahinozzaman M, et al. Long non-coding RNAs in the doxorubicin resistance of cancer cells. *Cancer Lett* 2021;**508**:104−14.
44. Wang F, El-Saafin F, Ye T, Stierle M, Negroni L, Durik M, et al. Histone H2Bub1 deubiquitylation is essential for mouse development, but does not regulate global RNA polymerase II transcription. *Cell Death Differ* 2021;**28**:2385−403.
45. Duijf PHG, Nanayakkara D, Nones K, Srihari S, Kalimutho M, Khanna KK. Mechanisms of genomic instability in breast cancer. *Trends Mol Med* 2019;**25**:595−611.
46. Gifford JB, Hill R. GRP78 influences chemoresistance and prognosis in cancer. *Curr Drug Targets* 2018;**19**:701−8.
47. Luo J, Xia Y, Yin Y, Luo J, Liu M, Zhang H, et al. ATF4 destabilizes RET through nonclassical GRP78 inhibition to enhance chemosensitivity to bortezomib in human osteosarcoma. *Theranostics* 2019;**9**:6334−53.
48. Chen S, Wu J, Jiao K, Wu Q, Ma J, Chen D, et al. MicroRNA-495-3p inhibits multidrug resistance by modulating autophagy through GRP78/mTOR axis in gastric cancer. *Cell Death Dis* 2018;**9**:1070.
49. Tsai YL, Ha DP, Zhao H, Carlos AJ, Wei S, Pun TK, et al. Endoplasmic reticulum stress activates SRC, relocating chaperones to the cell surface where GRP78/CD109 blocks TGF-β signaling. *Proc Natl Acad Sci U S A* 2018;**115**:E4245−54.

50. Clarke WR, Amundadottir L, James MA. CLPTM1L/CRR9 ectodomain interaction with GRP78 at the cell surface signals for survival and chemoresistance upon ER stress in pancreatic adenocarcinoma cells. *Int J Cancer* 2019;**144**:1367−78.
51. Sriratanasak N, Chunhacha P, Ei ZZ, Chanvorachote P. Cisplatin induces senescent lung cancer cell-mediated stemness induction *via* GRP78/Akt-dependent mechanism. *Biomedicines* 2022;**10**:2703.
52. Wu CP, Hsiao SH, Wu YS. Perspectives on drug repurposing to overcome cancer multidrug resistance mediated by ABCB1 and ABCG2. *Drug Resist Updat* 2023;**71**:101011.
53. Li W, Tibben M, Wang Y, Lebre MC, Rosing H, Beijnen JH, et al. P-glycoprotein (MDR1/ABCB1) controls brain accumulation and intestinal disposition of the novel TGF-β signaling pathway inhibitor galunisertib. *Int J Cancer* 2020;**146**:1631−42.